AFRL-AFOSR-UK-TR-2012-0056

Attenuation of Cavity Bay Noise

Professor David G. MacManus

Cranfield University
School of Engineering
Department of Power and Propulsion
Cranfield, United Kingdom MK43 0AL

EOARD Grant 11-3025

Report Date: October 2012

Final Report for 01 September 2011 to 31 August 2012

Air Force Research Laboratory
Air Force Office of Scientific Research
European Office of Aerospace Research and Development
Unit 4515 Box 14, APO AE 09421

REPORT DOCUMENTATION PAGE

Form Approved OMB No. 0704-0188

1. REPORT DATE *(DD-MM-YYYY)*	2. REPORT TYPE	3. DATES COVERED *(From – To)*
01 October 2012	Final Report	1 September 2011 – 31 August 2012

4. TITLE AND SUBTITLE

Attenuation of Cavity Bay Noise

5a. CONTRACT NUMBER

FA8655-11-1-3025

5b. GRANT NUMBER

Grant 11-3025

5c. PROGRAM ELEMENT NUMBER

61102F

6. AUTHOR(S)

Professor David G. MacManus

5d. PROJECT NUMBER

5d. TASK NUMBER

5e. WORK UNIT NUMBER

7. PERFORMING ORGANIZATION NAME(S) AND ADDRESS(ES)

Cranfield University
School of Engineering
Department of Power and Propulsion
Cranfield, United Kingdom MK43 0AL

8. PERFORMING ORGANIZATION REPORT NUMBER

N/A

9. SPONSORING/MONITORING AGENCY NAME(S) AND ADDRESS(ES)

EOARD
Unit 4515 BOX 14
APO AE 09421

10. SPONSOR/MONITOR'S ACRONYM(S)

AFRL/AFOSR/EOARD

11. SPONSOR/MONITOR'S REPORT NUMBER(S)

AFRL-AFOSR-UK-TR-2012-0056

12. DISTRIBUTION/AVAILABILITY STATEMENT

Approved for public release; distribution is unlimited. (approval given by local Public Affairs Office)

13. SUPPLEMENTARY NOTES

14. ABSTRACT

This report concludes the investigation into the attenuation of cavity bay noise conducted under EOARD Award number FA8655-11-1-3025. A preliminary report was provided to EOARD in April 2012 and can be considered in conjunction with this final report. This investigation covers the experimental analysis and the development of passive palliative devices at both 1/40th and 1/20th scale and under both subsonic and supersonic conditions. Two methods of attenuation are of interest. The first is a resonant array based on the principle similar to that of a Helmholtz resonator and the second is a device comprised of a porous wire mesh coupled with a confined backing volume. The resonant arrays provide a source of viscous losses which can be targeted at the frequencies of the Rossiter modes within the cavity and the porous mesh devices provide viscous losses over a broader range of frequencies.

15. SUBJECT TERMS

EOARD, Cavity Acoustics, Aerodynamics

16. SECURITY CLASSIFICATION OF:			17. LIMITATION OF ABSTRACT	18, NUMBER OF PAGES	19a. NAME OF RESPONSIBLE PERSON
a. REPORT	b. ABSTRACT	c. THIS PAGE			Gregg Abate
UNCLAS	UNCLAS	UNCLAS	SAR	50	19b. TELEPHONE NUMBER *(Include area code)* +44 (0)1895 616021

Attenuation of Cavity Bay Noise
Final report

FA8655-11-1-3025

September 2012

David Roberts
Dr David MacManus
Department of Power and Propulsion
School of Engineering
Cranfield University

Executive Summary

This report concludes the investigation into the attenuation of cavity bay noise conducted under EOARD Award number FA8655-11-1-3025. A preliminary report was provided to EAORD in April 2012 and can be considered in conjunction with this final report. This investigation covers the experimental analysis and the development of passive palliative devices at both 1/40th and 1/20th scale and under both subsonic and supersonic conditions. Two methods of attenuation are of interest. The first is a resonant array based on the principle similar to that of a Helmholtz resonator and the second is a device comprised of a porous wire mesh coupled with a confined backing volume. The resonant arrays provide a source of viscous losses which can be targeted at the frequencies of the Rossiter modes within the cavity and the porous mesh devices provide viscous losses over a broader range of frequencies.

This report contains background information on both the cavity bay noise characteristics and the design process associated with the resonant array palliatives. Designs are presented for 1/40th scale tests which have been conducted at Cranfield University and also for 1/20th scale tests which were conducted with a generic 1/20th scale cavity model installed into the Trisonic Gasdynamics facility at Wright Patterson Air Force Base. The effect of the high sound pressure environment within a resonant cavity on the performance of resonant arrays has also been investigated and a new model has been developed. The aim of this new model is to capture the non-linear effects that the high pressure environment imparts on the arrays.

The most important results from the medium scale (1/20th) tests indicate that resonant arrays can be used to provide attenuation levels of up to 26dB within a cavity under supersonic (Mach 1.5) conditions. This is a new finding, which demonstrates the potential of resonant arrays as palliatives within the supersonic regime where typical spoiler type devices are less reliable. The design rules taken from the small scale tests enabled arrays to be designed to target modes within a supersonic cavity and, much like small scale devices, a combined configuration with an array installed at both cavity ends provided an attenuation of up to 15dB at multiple modes simultaneously.

Results from the 1/40th scale tests demonstrate that resonant arrays can provide up to 15dB attenuation at the second mode and 19dB attenuation at the third Rossiter mode for Mach 0.9 flows. The results also provide support for the rules, specifically the relationship between attenuation and array resistance, used in the design process of the resonant arrays used for the 1/20th scale tests. An additional 1/40th scale investigation assessed the performance of porous mesh based devices and attenuations of around 12dB have been demonstrated.

This report also investigates the phenomena of mode switching within the cavity flow as this is thought to be associated with unwanted modal amplification, known as peaking. Overall, the palliative devices based on resonant arrays have demonstrated high levels of attenuation which are comparable to more conventional acoustic control techniques. It is expected that whilst the devices perform well under subsonic conditions the main operational role of the devices could be as supporting palliatives. These would be used to improve attenuation performance within the supersonic regime, where typical attenuation devices often fail to provide the required level of attenuation.

Table of Contents

List of Figures

List of Tables

1 Introduction

The main focus of this report is the attenuation results from medium (1/20th) scale tests carried out under EOARD award number FA8655-11-1-3025. The current final report provides a summary of the cavity noise issue and a description of the proposed palliative devices. In this report, the term "palliative" is used as a general term to describe the flow control devices or attenuators used within the cavity. This report is to be used in conjunction with an interim report which was submitted to EOARD in April 2012 [1].

1.1 Cavity noise background

The majority of modern military aircraft, including recent UCAV designs, are designed with internal stores carriage. Housing stores within a weapon bay cavity has the two fold benefit to the aircraft of reduced excrescence drag and a smaller radar signature. However, an open cavity exposed to an external flow can result in modal unsteady pressure fluctuations [2], which can reach intensities of up to 160dB [3]. High intensity pressure fluctuations can cause damage to both the aircraft and any sensitive components carried within the open weapon bay.

Flow over cavities can be broadly categorised into two regimes which are referred to as open and closed flows [4]. For open flow, the shear layer bridges the cavity and reattaches at the cavity rear wall (RW). For this flow field, vortices are convected downstream from the cavity front wall (FW) and impinge at the rear wall stagnation point. The upstream propagation of unsteady pressure waves within the cavity is a result of this convective process [2] [4]. For closed flow, the shear layer reattaches on the cavity ceiling and the high intensity pressure fluctuations are predominantly avoided. However, closed flow cavities often exhibit strong adverse pressure gradients which can affect store release characteristics and are usually avoided. A typical open flow cavity will have a length (l) to depth (h) ratio of less than 6 and a closed flow cavity will typically have an l/h greater than 10 [4]. This work concentrates on cavities which exhibit open flow characteristics, where the acoustic spectra typically exhibit high intensity modal peaks (*Figure 1*). The frequencies at which the peak intensities occur correspond to values predicted by *Equation 1* [5] and are generally known as Rossiter frequencies.

$$St = \frac{fl}{U_\infty} = \frac{m - \alpha}{M_\infty \left(1 + \frac{\gamma - 1}{2} M_\infty^2\right)^{-\frac{1}{2}} + \frac{1}{k}} \qquad \textbf{Equation 1}$$

In this expression (*Equation 1*) α and k are empirical constants. α is a function of the cavity aspect ratio (l/h) and relates the phase of the shed vortices in the shear layer to the propagation of the pressure wave within the cavity. The constant k relates the speed of the vortex convection in the shear layer to the velocity of the freestream flow and is a function of the freestream Mach number. For this current study these parameters were taken as α = 0.062l/h and k = 0.57 [2]. The value of U_∞ was calculated from the ratio of the derived tunnel Mach number, based on the ratio of the tunnel static and total pressures, and the local speed of sound. This sound speed was calculated from the tunnel static temperature, which was derived using the isentropic relationship between the ratio of static to total temperature and the tunnel Mach number.

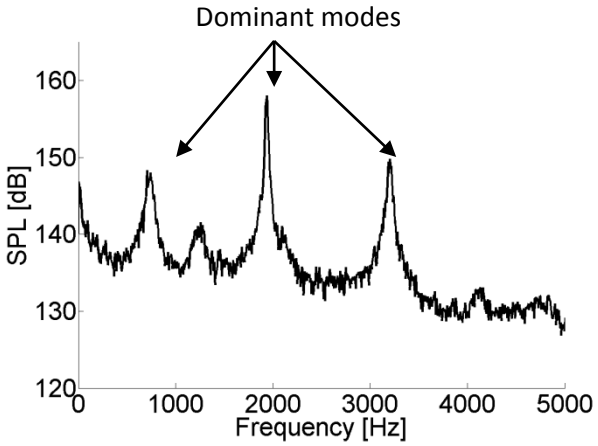

Figure 1 – A typical cavity modal acoustic spectrum at 1/40th scale (Mach 0.9)

1.2 Methods of attenuation

Because of the potential for damage to aircraft and stores, various palliative methods have been developed. These devices have encompassed both active and passive methods under both transonic and supersonic conditions [6] [7] [8]. These studies indicate that peak attenuations of 20dB and 30dB can be achieved by passive and active devices respectively. The most common device currently in use is a spoiler placed upstream of the cavity. This is designed to disrupt the airflow over the cavity and break the feedback mechanism associated with the generation of the modal peaks.

Within this report the attenuation performances from two palliative devices are discussed, the first device is an array of Helmholtz type resonators and the second is a porous mesh device. Results from 1/40th scale tests which have previously been reported [1] will be summarised and an account of the main findings from 1/20th scale tests are provided.

The first palliative to be investigated is a device based on the properties of Helmholtz resonators [9] [10]. A Helmholtz type resonator is formed from an enclosed backing volume with an elongated neck open at both ends. When excited, the air within the neck vibrates. A maximum displacement and therefore attenuation is reached when the resonant frequency condition is met. The attenuation from a Helmholtz type resonator is achieved through frictional losses, vortex shedding and the effective damping action of the air within the backing cavity. Viscous losses also occur in the neck region. Throughout this report this palliative device is referred to as a resonator or a resonant array.

The resonant arrays used in the current study consist of multiple orifices coupled with a common backing volume. Each orifice represents a single Helmholtz resonator unit and a sketch of two adjacent orifices is shown in *Figure 2*a along with the design variables used to design and to tune the arrays. This arrangement behaves in a similar way to individual Helmholtz resonators and can provide a similar tuned attenuation [11] [12]. In this study the orifices were formed by a cylindrical hole drilled through a sheet faceplate and the backing volume was formed from a sealed box structure.

A second type of passive palliative, formed from a porous wire mesh and backing volume, will also be investigated (*Figure 2 b*). This device is expected to provide broadband attenuation and not the targeted attenuation provided by resonant arrays. The mesh based devices absorb energy from the cavity flow field by allowing the passage of the high intensity pressure waves within the cavity through its surface. Attenuation is caused by the viscous losses that occur within the open structure of the porous mesh. Typically the backing length (L (*Figure 2 b*)) is set to correspond to the condition $L=\lambda/4$, where λ corresponds to the wavelength of the target disturbance. The $\lambda/4$ condition maximises the particle velocity through the porous mesh and is designed to yield the greatest attenuation. Due to size constraints placed on installations within aircraft cavities it is unlikely that

the λ/4 condition can be fulfilled and therefore porous mesh devices may not be able to provide a high level of attenuation.

Resonant arrays offer a simple and robust technique for the attenuation of cavity modes. These palliative devices can be installed inside the weapon bay cavity and will not add excrescence drag or the requirement for actuation to the parent aircraft, unlike with spoilers or active attenuation methods.

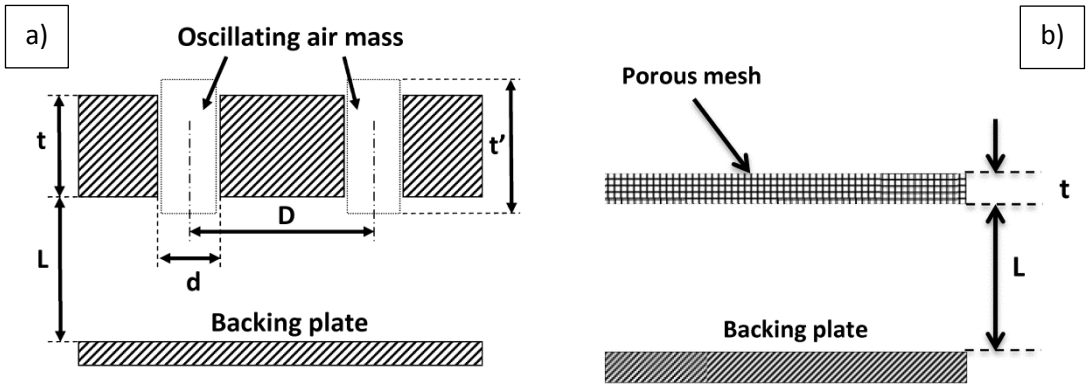

Figure 2 -- Schematic arrangement of a) perforated plate with a common backing volume, b) porous wire mesh device

2 Methods, Assumptions, and Procedures

2.1 Summary of wind tunnel facilities used within this investigation

Two wind tunnel facilities were used for the cavity palliative investigations within this body of work. The first facility provided the opportunity to test palliative devices within a small (1/40th) scale cavity at high subsonic Mach numbers (Mach 0.8 to 0.95). The second facility enable palliative performance to be tested within a medium (1/20th) scale cavity at both Mach 0.7 and 1.5. The ability to test the devices under supersonic (Mach 1.5) conditions was important as this could not have been achieved using the initial small scale facility.

This section also provides information about the acoustic and geometric properties of the various palliative devices which were tested at both scales. A summary of the attenuation results for all of the palliative device configurations is provided in APPENDIX A.

2.1.1 Small scale 1/40th wind tunnel tests

The initial small scale wind tunnel tests were conducted using the Cranfield University 2.5" tri-sonic wind tunnel. The cavity has a length (l) of 100mm, depth (h) of 20mm and a width (w) of 25mm. This cavity therefore has an l/h ratio of 5 placing it into the open flow regime and this has been confirmed in previous work where the cavity exhibited resonant characteristics with modal peaks occurring around 800Hz, 2.0kHz and 3.2kHz [11]. A full description of this facility and the data acquisition process are provided in the interim report which was submitted in April 2012 [1].

2.1.1.1 Parts designed for small scale (1/40th) wind tunnel tests

There has been previous experience in the design process behind resonant array based palliatives specifically at small scale [11]. The main interests of the EOARD funded tests within this report were to assess whether small scale design rules could be applied to a medium scale cavity and also to investigate the attenuation performance of resonant arrays under supersonic conditions.

For the initial stages of the investigation into the use of resonant arrays for the attenuation of weapon bay cavity acoustics two resonant devices were designed alongside three porous mesh type

devices. The resonant arrays were designed to provide a specified impedance level at the faceplate [1] and the mesh devices were designed based on results from impedance tube testing [1].

ARRAY A was designed to exhibit a predicted normalised resistance within the optimum range 0.25 < Re(Z)* < 0.60 at the frequency of the second mode (2kHz) [1]. The geometric and predicted acoustic properties are given in *Table 1* and the array can be seen installed into the model cavity in *Figure 3*. The array exhibits a normalised resistance of Re(Z)*=0.33 which places it within the range which is expected to yield a high level of attenuation [1]. The porosity (ε) of the array (8.7%) matches that of another array which has been previously tested and has demonstrated a high level of attenuation [11]. The α and β values also match closely to successful arrays. *ARRAY A* has been specifically designed to target the design point for arrays which target the second cavity mode and is therefore expected to provide a large level of attenuation at the second cavity mode (2kHz).

ARRAY B has been designed to target the third cavity mode which has a frequency of around 3.2kHz (*Figure 1*). The geometric and predicted acoustic properties are given in *Table 1*. This array (*ARRAY B*) has a lower predicted normalised resistance (Re(Z)*) value when compared with other successful third mode arrays and the other parameters (β, α, and ε) closely match other successful arrays which also targeted the third mode. *ARRAY B* is expected to provide a useful amount of attenuation at the third mode only, broadband noise and OASPL are not expected to be affected by the installation.

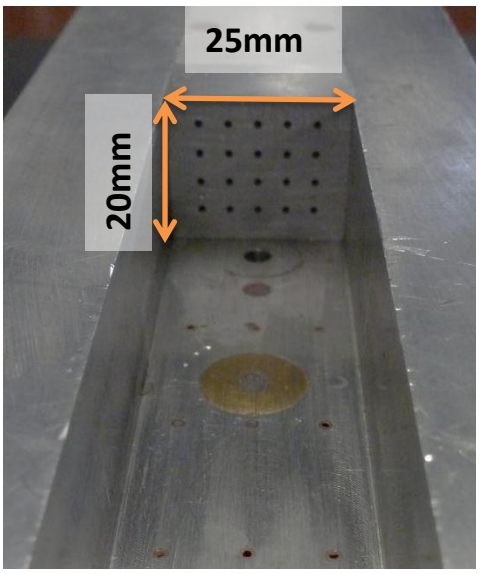

Figure 3 – *ARRAY A* installed into the cavity model end wall

	d (mm)	D (mm)	t (mm)	L (mm)	ε (%)	Peak α	β (%)	Re(z)*
ARRAY A	1	3	7	8	8.7	0.74	38	0.33
ARRAY B	5	7	4	11	40.1	0.08	69	0.02

Table 1 – Geometric and predicted acoustic properties for small scale *ARRAY A* and *B*

2.1.1.2 Porous wire mesh devices

Three porous wire mesh based devices were designed for the 1/40th scale tests. Each device shares a common porous faceplate, but the properties of the backing cavity differ to assess the impact of ventilation on the attenuation performance of the porous mesh devices. The geometric and acoustic properties of the arrays are given in *Table 2*. *MESH A* has been designed with the same dimensions as the array which was tested using an impedance tube [1] to assess its acoustic properties and is formed from a porous faceplate coupled with a non-ventilated backing volume (*Figure 4a*). *MESH B* and *MESH C* are formed from a porous faceplate coupled with a backing volume which has a ventilated surface open to the freestream flow (*Figure 4b*). All three mesh devices are expected to provide broadband attenuation with the greatest attenuation at higher frequencies (above 3kHz).

	Mesh ε (%)	L (mm)	Ventilation ε (%)	Empirical faceplate Re(z)*
MESH A	53	13.2	0	0.3
MESH B	53	13.2	8.7	0.3
MESH C	53	13.2	29	0.3

Table 2 – Geometric and acoustic properties of the small scale MESH devices

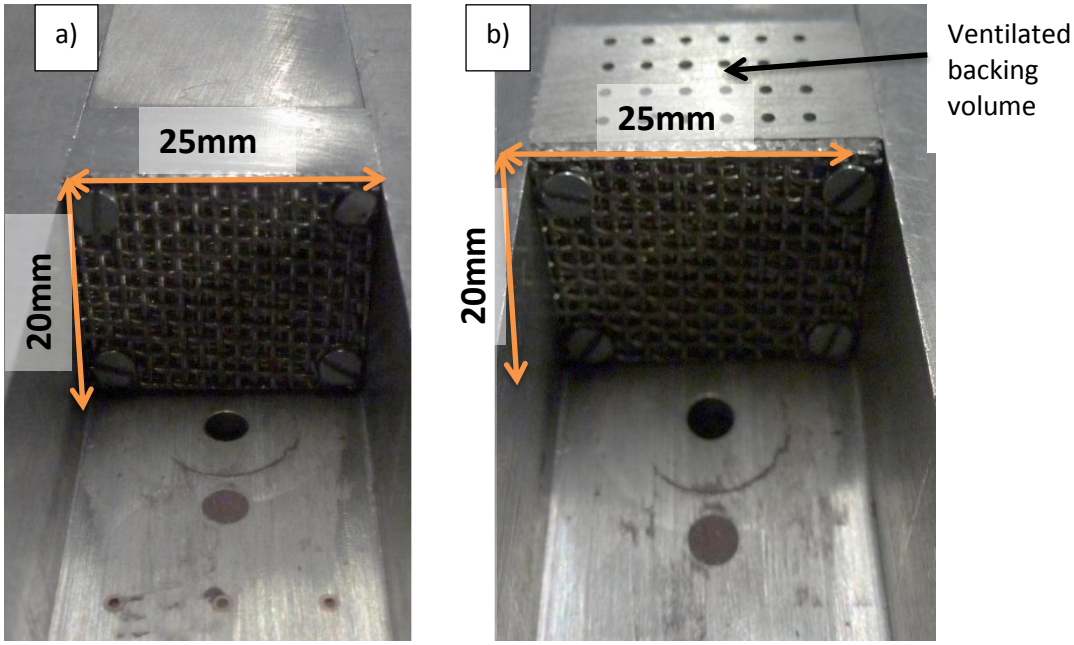

Figure 4 – a) Porous mesh device with non-ventilated backing volume (*MESH A*) installed into cavity model, b) Porous mesh device with 8.7% porosity ventilated backing volume (*MESH B*) installed into cavity model.

2.1.2 Medium scale 1/20th wind tunnel scale tests

A series of wind tunnel tests were completed with a generic 1/20th scale cavity model installed into the TGF at Wright Patterson Air Force Base (*Figure 5a, b, c*). These tests were designed to support the main objectives of the investigation and to provide additional research opportunities which are not available within the facilities at Cranfield University. The additional opportunities include the ability to test the palliatives in a larger 1/20th scale model and also to test the attenuation performance under supersonic freestream conditions (Mach 1.5).

The 1/20th scale cavity model houses a cavity with length l=216mm, depth h=38mm and width w=64mm (*Figure 5c*). This results in a cavity with a length to depth aspect ratio of l/h=5.6 which places it within the open flow criteria for a modal cavity environment [5]. Palliative devices can be installed in either the front or rear wall of the cavity. A full description of this facility and the data acquisition procedures are provided in the interim report which supports this document [1].

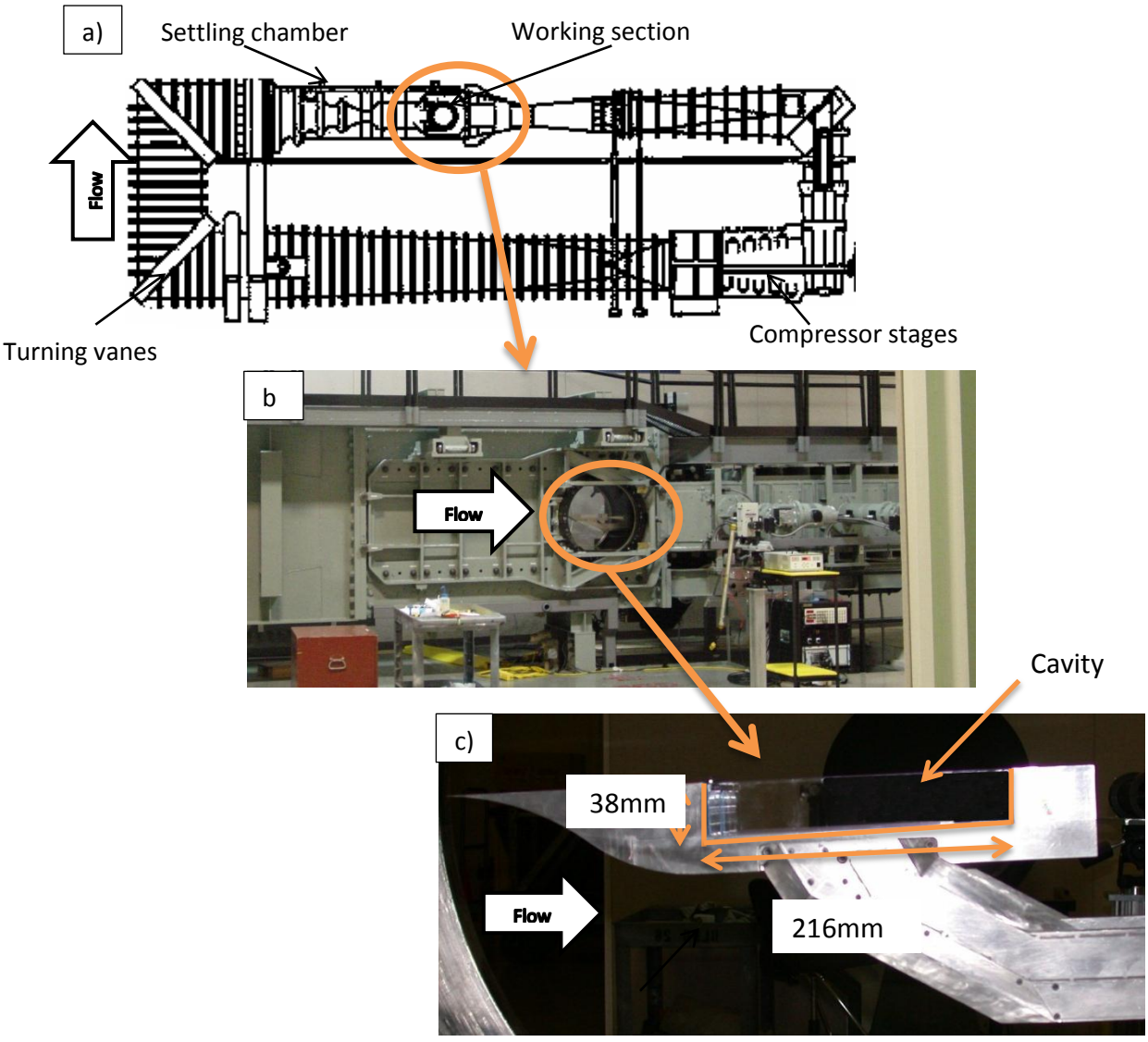

Figure 5 –a) Schematic diagram of TGF [13] , b) TGF working section, c) ADDICT cavity model installed into TGF.

2.1.2.1 Parts designed for the medium (1/20th) scale wind tunnel tests

The tests planned for the medium scale cavity were designed to investigate both resonant array and porous mesh based palliatives at Mach 0.7 and Mach 1.5. Details of how the palliative were installed into the cavity model can be found in the supporting interim report [1].

A series of seven resonant arrays were designed for the 1/20th scale cavity model to be tested at Mach 0.7 within the TGF. These arrays were designed following rules which were developed in the small scale tests [1] and the tests are designed to examine whether these rules can be extrapolated to medium scale. The geometric and predicted acoustic properties of the arrays are given in *Table 3*. TGF_0.7_1 and TGF_0.7_2 target the second and third modes respectively. These two arrays have been designed to demonstrate similar resistance (Re(Z)*) properties when compared to the most successful devices tested previously at 1/40th scale [11]. It is expected that both arrays will provide a useful amount of attenuation at their respective modal frequencies. TGF_0.7_1 has a normalised resistance of 0.31 which places it within the recommended range for high attenuation at the second mode based on the 1/40th scale tests. TGF_0.7_2 has a low faceplate normalised resistance (Re(Z)*) value of 0.05 which places it within the recommended range for high attenuation at the third mode. TGF_0.7_3, TGF_0.7_4, TGF_0.7_5, and TGF_0.7_6 have been designed to target the second mode and have a normalised resistances over the range 0.22 <Re(Z)*<0.57. These arrays have been designed to provide a group of arrays with resistance values that span the recommended range based on the tests conducted at 1/40th scale. TGF_0.7_7 has been designed to target the third mode and has a normalised resistance which lies on the upper boundary of the recommended range for attention at the third cavity mode. All of the arrays are expected to provide a useful amount of attenuation at their target modes and the tests will reveal the optimum level of resistance required for an array to yield a large attenuation.

Array	Mode frequency (Hz)	d (mm)	D (mm)	t (mm)	L (mm)	ε (%)	α	β (%)	Re(Z)*
TGF_0.7_1	2nd (800)	1.7	7.1	8.7	17.3	4.7	0.73	35	0.31
TGF_0.7_2	3rd (1300)	5.2	11.9	6.9	19.1	14.9	0.17	48	0.05
TGF_0.7_3	2nd (800)	2	10	4	19	3.1	0.6	35	0.22
TGF_0.7_4	2nd (800)	2	9	11	12	3.9	0.8	25	0.38
TGF_0.7_5	2nd (800)	2	10	12	9	3.1	0.9	21	0.52
TGF_0.7_6	2nd (800)	1	7	3	15	1.6	0.93	36	0.57
TGF_0.7_7	3rd (1300)	2	8	8	8	4.9	0.7	24	0.30

Table 3 – Summary of resonant arrays designed for the 1/20th scale cavity model at Mach 0.7

Due to the large difference in modal frequencies exhibited at Mach 0.7 and Mach 1.5 (*Table 3* and *Table 4*) a new set of arrays were required to attenuate the cavity modes at Mach 1.5. The geometric and predicted acoustic properties for the four arrays designed for the Mach 1.5 test cases are summarised in *Table 4*. TGF_1.5_1 and TGF_1.5_2 target the second and third modes respectively and have been designed to demonstrate similar resistance (Re(Z)*) properties compared with the most successful cases at 1/40th scale. Because of the increased frequency of the modes at Mach 1.5 the porosity (ε) of the arrays was increased to allow for the arrays to be tuned to the higher modal frequencies at Mach 1.5 whilst maintaining geometrically scaled d, t, and L dimensions. TGF_1.5_3 was designed to produce an array which targets the second mode with a normalised resistance of 0.51. This resistance value is within the recommended range from the 1.40th scale tests [1]. TGF_1.5_4 was designed to produce an array to target the third mode with a low ε and small installation footprint (t+L/l=3.2%). *Figure 6a* shows TGF_1.5_1 installed into the front wall of the ADDICT cavity model.

Array	Mode frequency (Hz)	d (mm)	D (mm)	t (mm)	L (mm)	ε (%)	α	β (%)	Re(Z)*
TGF_1.5_1	2nd (1200)	1.7	4.8	8.7	17.3	10.2	0.51	46	0.17
TGF_1.5_2	3rd (1900)	5.2	8	6.9	19.1	33	0.10	70	0.03
TGF_1.5_3	2nd (1200)	1	6	3	10	2.2	0.89	33	0.51
TGF_1.5_4	3rd (1900)	2	10	2	5	3.1	0.60	22	0.23

Table 4 – Summary of resonant arrays deigned for the 1/20th scale cavity model at Mach 1.5

A set of three porous mesh type devices were tested within the 1/20th scale cavity. These devices are formed in a similar way to the 1/40th scale mesh devices where a porous faceplate is coupled with a confined backing volume. A summary of the mesh devices is given in *Table 5*. Two mesh faceplates will be used for the arrays, one exhibits a low resistance (Re(Z)*=0.3) and the second exhibits a higher resistance (Re(Z)*=1.5). The difference in the attenuation exhibited by these two devices should highlight the effect that the resistance terms has on the attenuation mechanism for a porous mesh device and it would be expected that a device with a higher resistance (Re(Z)*) would provide the greater attenuation level.

The porous mesh devices will be tested at both Mach 0.7 and Mach 1.5 with no modifications as their attenuation should not demonstrate the same level of sensitivity to the frequency changes compared to a resonant array type design. The effect of ventilation from the backing volume into the freestream flow will also be investigated at the larger 1/20th scale. *Figure 6b* demonstrates TGF_m3 installed in the rear wall of the ADDICT cavity model.

Mesh device	Re(Z)*	Ventilation ε (%)
TGF_m1	1.5	0
TGF_m2	0.3	0
TGF_m3	0.3	50

Table 5 – Summary of the porous mesh devices designed for the 1/20th scale cavity model

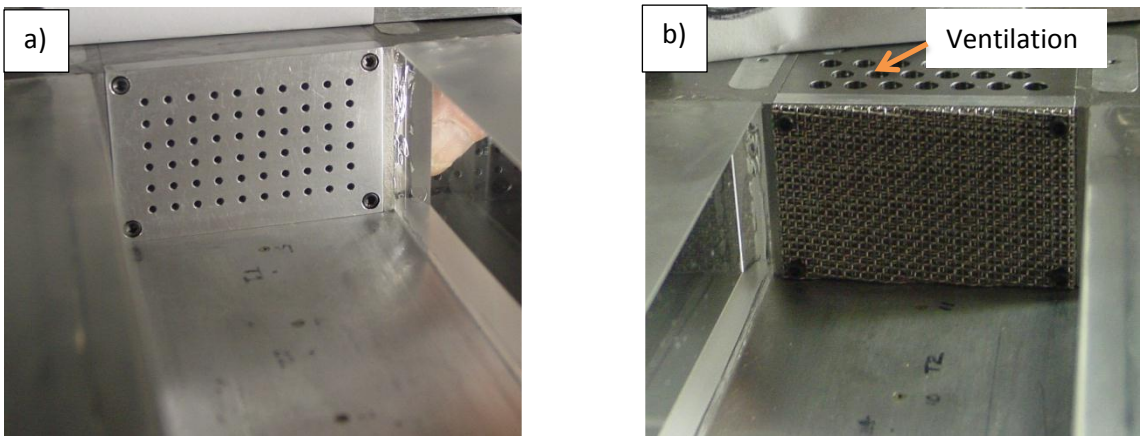

Figure 6 – a) TGF_1.5_1 installed in the ADDICT cavity front wall, b) TGF_m3 installed in the ADDICT cavity rear wall

2.2 Analytical model for array design in the high SPL cavity environment

The impedance of an array (HSPL_ARRAY #1 (*Table 6*)) was investigated under high SPL conditions using an impedance tube [1]. The impedance tube tests yield an empirical measure of both the array's absorption coefficient (α) and impedance values (Z*). This allows for a comparison to be made between empirical results and the profiles predicted by the analytical model. *Figure 7* demonstrates that the analytical model can predict the resonant frequency of an array to within ±4% for SPL up to 155dB. This is around the SPL which is typically expected within resonant weapon bay cavities. However, at an SPL of 155dB the analytical model underpredicts the absorption coefficient by around 30%. The reason for this becomes apparent when the impedance values of the array are investigated. The analytical model demonstrates a good correlation with the empirical results for the prediction of the array's reactance (*Figure 8a)*. However, the analytical model underpredicts the resistance of the array by around 50% at an SPL of 155dB (*Figure 8b*). This under prediction of the resistance explains the difference between the predicted absorption coefficient and that measured at 155dB. The increase in resistance caused by the high SPL environment must be taken into account when designing resonant arrays. If the resistance of an array increases beyond unity then the attenuation performance may suffer as the device will move away from the ideal condition. The following section will discuss how the analytical model used for the array design may be improved to better account for the effects of the high SPL cavity environment.

Array name	Target mode	f (Hz)	d (mm)	D (mm)	t (mm)	L (mm)	ε (%)	α_{max}	β (%)	R/ρc
HSPL_ARRAY #1	2nd	1942	1	3	5	10	8.7	0.63	46	0.25

Table 6 – Geometric and acoustic properties of the resonant array used for high SPL investigation of the analytical model reliability

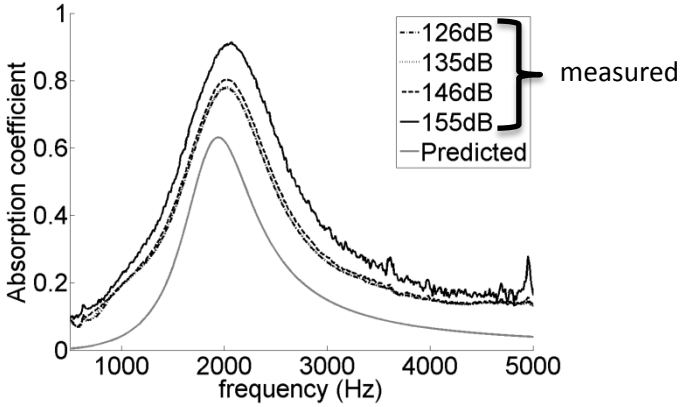

Figure 7 – Effect of SPL on Absorption coefficient

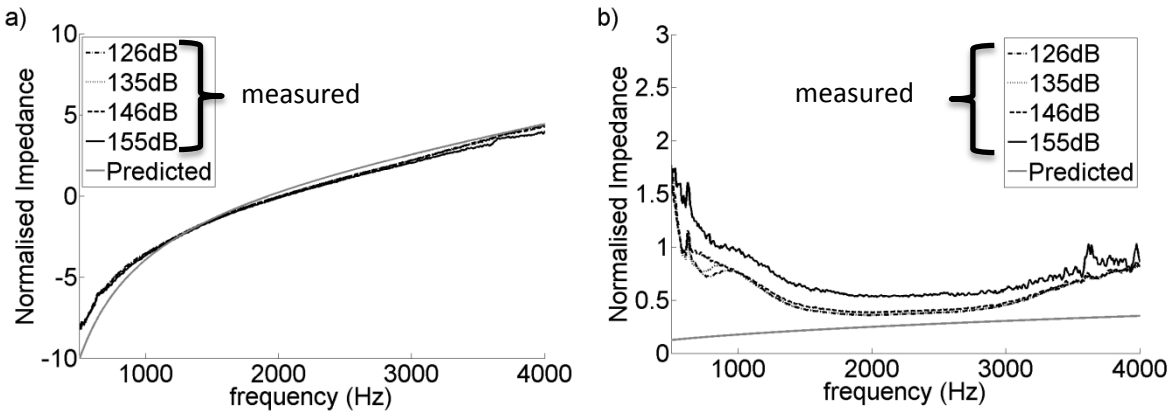

Figure 8 – a) Effect of SPL on reactance, b) Effect of SPL on resistance (resonant frequency ≈2kHz)

2.2.1 Defining the non-linear regime for a resonant array

There are various parameters which can be used to define the non-linear behaviour of an array. A typical rule of thumb is to treat any SPL above 100dB as causing some degree of non-linear behaviour [14]. Also non-linear resistance characteristics are also expected when the displacement of the oscillation within the orifice is of the same order as the orifice diameter [15]. Typically, at higher SPL intensities the Reynolds number of the flow through the orifice increases beyond the laminar flow threshold (Re_d>2000) which contributes to the increase in the array resistance through skin friction increases within the orifice. The orifice velocity is calculated from the acoustic particle velocity which is linked to the SPL (*Equation 2* and *3*), where p_{ref} is the standard reference pressure for SPL ($2x10^{-5}$Pa), u_n is the particle velocity in front of the orifice, and u_o is the velocity through the orifice.

The calculated increase in the Reynolds number agrees with previous work which linked an increase in energy losses through an orifice to the increase in the values of the convective flow terms [16]. This previous work [16] provides the parameters set out in *Equation 4* and *Equation 5* to assess whether an array will be operating in the linear or non-linear regime. These equations are related to the ratio of momentum convection to shear (*Equation 4*) and inertia (*Equation 5*), where the momentum convection is linked to the particle velocity through the orifice (u_o) and ω is the rotational frequency of the device calculated from the resonant frequency of the array. The resultant parameters have been calculated for HSPL_ARRAY #1 (*Table 7*) and the results are therefore pertinent to the small scale tests. It is expected that if only one of the parameters is greater than unity that the array will exhibit slight non-linear properties, but the resistance will remain predominantly linear. This was seen for the 126dB to 146dB HSPL_ARRAY #1 cases [1]. However, when both parameters are greater than one the array will exhibit highly non-linear characteristics. This highly non-linear behaviour was exhibited by HSPL_ARRAY #1 for the measured resistance case at 155dB (Figure 8*b*) where there was a step increase in the array resistance when the SPL was increased from 146dB to 155dB and this agrees with the parameters in *Table 7*. Therefore, it has been confirmed that the behaviour of the resistance term (Re(Z)*) at high SPL is due to non-linear effects within the orifice of the array.

$$u_o = \frac{u_n}{\varepsilon} \qquad \textbf{Equation 2}$$

$$u_n = \frac{P_{ref}\left(10^{\frac{SPL}{20}}\right)}{\rho c} \qquad \textbf{Equation 3}$$

$$\frac{u_o}{\sqrt{\nu\omega}} > 1 \qquad \textbf{Equation 4}$$

$$\frac{u_o}{\omega d} > 1 \qquad \textbf{Equation 5}$$

SPL (dB)	Equation 4	Equation 5
126	2.3	0.1
135	7.4	0.3
146	23.4	0.8
155	73.9	2.6

Table 7 – Non-linearity parameters for HSPL_ARRAY #1 over the SPL range of 126dB to 155dB

2.2.2 Various models for resonant array performance within high SPL environments

This section discusses the acoustic properties calculated by various analytical models which have been proposed for use under high SPL conditions. The important term which accounts for the performance changes at high SPL was shown to be the array resistance (Figure 8*b*). The resistance of HSPL_ARRAY #1 is calculated using several analytical models and compared with the experimental data taken using the high SPL impedance meter. Finally, a new semi empirical model based on the findings from the high SPL analytical models is proposed.

2.2.2.1 The work of A. Guess [17]

The aim of this work was to produce a design method for single degree of freedom acoustic liners to be used within a high SPL environment. The focus of this work was to provide the design variables to achieve a prescribed reactance and resistance. The resistance term (Re(Z)*) was split into three constituent parts (*Equation 6*). The viscous term (*Equation 6*) corresponds to the resistance term used in the initial analytical model [1]. The two additional terms account for the increased resistance caused by the radiation of energy close to the orifice and the resistance due to non-linear interactions within the orifice. The radiation term is negligibly small (0.01% of the viscous term for HSPL_ARRAY_1) and is not expected to affect the final resistance value. However, the non-linear term is expected to be much greater than the viscous term under high SPL conditions (around 2000% of the viscous term) and this will provide the expected increase in the resistance at higher SPLs.

The non-linear term is related to the particle velocity within the orifices (u_o) and also to the Mach number of the flow through the orifices. The orifice velocity is calculated from the velocity normal to the faceplate u_n (*Equation 3*). The orifice velocity (u_o (*Equation 2*)) is expected to increase rapidly at high SPL intensities and this will greatly increase the resistance of the array when exposed to the high SPL environment. The K term in *Equation 6* is an empirical factor (taken as K=0.3 [17]) which is related to the thickness of the boundary layer over the surface of the perforated faceplate and M is the grazing flow Mach number. An increase in the boundary layer thickness over the plate would be expected to increase the K value.

Figure 9 shows a comparison between the experimental resistance values for HSPL_ARRAY #1 and those predicted using *Equation 6*. For the higher SPLs (155dB and 145dB) *Equation 6* over predicts the resistance by around a factor of two and for the lower SPLs (135dB and 125dB) *Equation 6* under predicts the resistance by around 25%. Therefore, this method is unacceptable for the prediction of the effects of high SPL on the performance of HSPL_ARRAY #1. This may be due to the relatively low porosity (ε=8.7%) of HSPL_ARRAY #1 compared with the ε=33% example used in the literature. The quiescent conditions of the impedance tube where there is no grazing flow over the device is not expected to cause this discrepancy as with a value of K=0.3 the grazing flow interaction term is expected to only add a normalised resistance of around 2×10^{-4}.

$$\mathrm{Re}(Z)^* = \frac{1}{\rho c}\left[\underbrace{\frac{\sqrt{8\upsilon\omega}}{\varepsilon c}\left(1+\frac{t}{d}\right)}_{\text{viscous}} + \underbrace{\frac{\pi^2}{2\varepsilon}\left(\frac{d}{\lambda}\right)^2}_{\text{radiation}} + \underbrace{\frac{\left(1-\varepsilon^2\right)}{\varepsilon}\left(\frac{|u_o|}{c}+KM\right)}_{\text{Non-linear}}\right] \qquad \textbf{Equation 6}$$

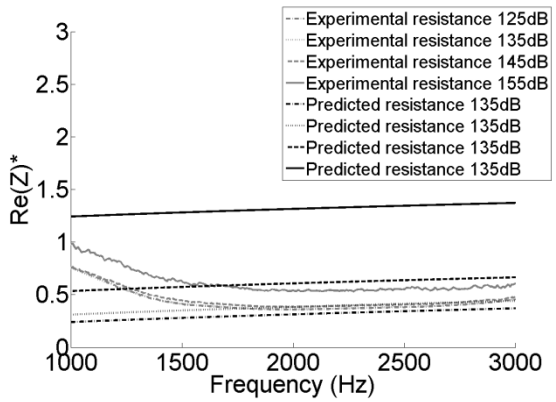

Figure 9 – Experimental and predicted resistance (Re(Z)*) for HSPL_ARRAY #1 using the Guess model [17] over the SPL range 125dB to 155dB

2.2.2.2 The work of D. Maa [18]

The focus of this work was to produce an analytical model capable of capturing the non-linear behaviour of micro-perforated arrays under high SPL conditions. Typically micro-perforated arrays have a low porosity (ε) and an orifice diameter (d) of the order of 1mm or less. Therefore, with a value of d=1mm and a relatively low ε it was expected that whilst this model would provide a good representation of the resistance properties of HSPL_ARRAY #1.

To capture the non-linear behaviour of the array an extra term was added to the resistance equation (*Equation 7*). The non-linear term relates the particle velocity (u_o) within the orifice to the pressure drop over the orifice. The non-linear term is then summed with the standard viscous resistance term to produce the total non-linear plate resistance. Again the non-linear resistance term is independent of the frequency of operation.

Figure 10 shows the comparison between the experimental resistance and the predicted resistance using *Figure 10*. At the higher SPL intensities (145dB and 155dB) the model over-predicted the resistance by around a factor of two and at the lower SPL intensities the model under predicted the resistance by around 25%. This is similar behaviour to the model discussed in the previous section (*Figure 9*) and may be again related to the porosity of HSPL_ARRAY #1. This model was designed for arrays with sub millimetre sized holes and porosity levels much lower than the ε=8.7% exhibited by HSPL_ARRAY #1. Therefore, the resistance predictions from this model are not acceptable for use as a performance guide.

$$\mathrm{Re}(Z)^* = \frac{1}{\rho c}\left[\frac{\sqrt{8\upsilon\omega}}{\varepsilon c}\left(1+\frac{t}{d}\right)+\frac{\rho|u_o|}{\varepsilon}\right] \qquad \textbf{Equation 7}$$

Non-linear

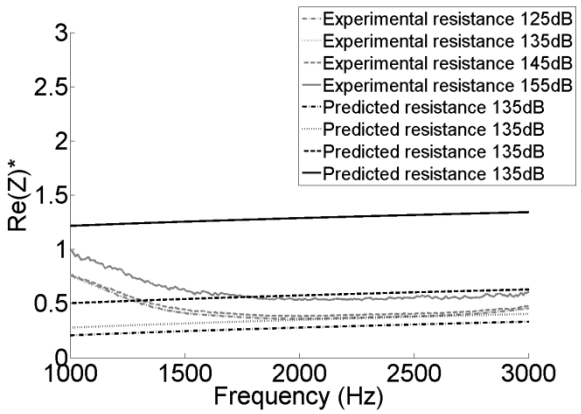

Figure 10 – Experimental and predicted resistance (Re(Z)*) for HSPL_ARRAY #1 using the Maa model [18] over the SPL range 125dB to 155dB

2.2.2.3 The work of Tayong and Leclaire [19]

Following the over prediction of the resistance from the previous two high SPL analytical models it was important to find a model that was designed and tested using arrays with similar characteristics to HSPL_ARRAY #1. The main aim of this work is to assess to what extent any interaction between the oscillating mass within one orifice interacts with the mass of an adjacent orifice, however a semi-empirical expression for the non-linear component of the resistance is also provided.

This study links the increase in the resistance to the Reynolds number of the flow through the orifice (Re_d (*Equation 9*)) using *Equation 8*. In *Equation 8* C_1 and C_2 are empirically determined constants taken as 0.049 and 0.98 respectively. The constants are used to fit a curve to the measured non-linear resistance of a model scale resonant array. Again the total resistance is the sum of the frequency dependant viscous term and the frequency independent non-linear term.

Figure 11 shows the experimental resistance values of HSPL_ARRAY #1 against frequency compared with the predicted values from *Equation 8*. For all SPL intensities (125dB to 155dB) this model under predicted the resistance of the array by around 25%. However, in contrast to the two previous models the under prediction was consistent over the SPL range. The important detail of this approach was the link between the Reynolds number and non-linear resistance. Due to the expected large increase in orifice velocity at the higher SPL intensities the Reynolds number undergoes a step change from being predominantly laminar to high transitional for the highest intensity (155dB). This behaviour is not sufficiently captured by this model due to the use of the empirical constants C_1 and C_2. The following section will discuss an improved semi-empirical approach for predicting the performance of resonant arrays under high SPL conditions.

$$\mathrm{Re}(Z)^* = \frac{1}{\rho c}\left[\frac{\sqrt{8\upsilon\omega}}{\varepsilon c}\left(1+\frac{t}{d}\right)+C_1\,\mathrm{Re}_d^{C_2}\right] \qquad \textbf{Equation 8}$$

Non-linear

$$\mathrm{Re}_d = \frac{\rho u_o d}{\mu} \qquad \textbf{Equation 9}$$

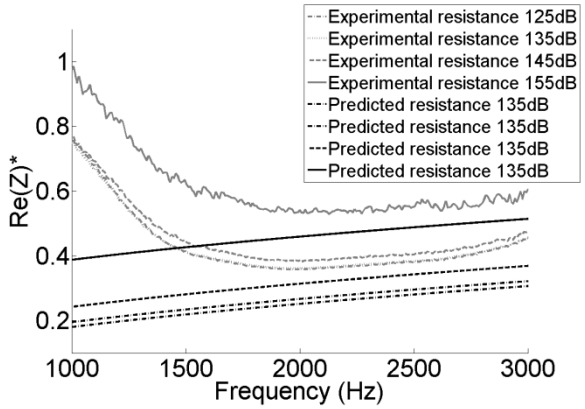

Figure 11 – Experimental and predicted resistance (Re(Z)*) for HSPL_ARRAY #1 using the Tayong & Leclaire model [19] over the SPL range 125dB to 155dB

2.2.3 A proposed semi-empirical model to predict array performance within the high SPL cavity environment

This section will discuss an improved semi-empirical approach for the prediction of the performance of resonant arrays under high SPL conditions. The previous sections demonstrated that the increase in the array resistance at high SPL intensity is linked to the Reynolds number of the flow through the orifice. However, the previous models did not accurately capture this behaviour for HSPL_ARRAY #1. Therefore, it was of interest to investigate the relationship between resistance (Re(Z)*) and the Reynolds number within an orifice (Re_d).

Figure 12 demonstrates that the resistance of HSPL_ARRAY #1 is directly proportional to the square of the Reynolds number (Re_d^2), based on the RMS particle velocity of the flow through the orifice. Therefore, the non-linear resistance of the array can be modelled by an equation of the form shown in *Equation 10* [19] where X is a non-dimensional constant and r is a constant resistance value for the minimum resistance under non-linear conditions (r=0.36 for SPL≥125dB (*Figure 12*)). To ensure that the resultant resistance is normalised to the characteristic impedance (Z_0=ρc) the constant X (*Equation 10*) is defined as the ratio of the freestream viscosity (μ) to the characteristic impedance (*Equation 11*). The final form of the updated non-linear resistance term ($Re(Z)^*_{NL}$) is given in *Equation 12* and this is added to the resistance from the initial analytical model [1] to provide the total resistance value (*Equation 13*). This (*Equation 12*) demonstrates the dependence of the non-linear resistance on the product of the Reynolds number (Re_d), Mach number (M) of the orifice flow as well as the orifice diameter (d).

Figure 13 demonstrates that this revised model (*Equation 13*) can capture the non-linear behaviour of the resistance of HSPL_ARRAY #1 over the SPL range 125dB to 155dB. *Equation 12* successfully captures the differing levels of resistance increase between the SPLs at the resonant frequency (1945Hz). This dependence of the resistance on both the Reynolds number and orifice Mach number was not correctly shown by the previous high SPL analytical models discussed previously in this section. Whilst this is an encouraging result it can only be tested for the HSPL_ARRAY #1 faceplate case as it was not possible to investigate the high SPL performance of other faceplate designs. Therefore, no comment can be given about the reliability of this approach when used for other resonant array designs.

$$\mathrm{Re}(Z)^*_{NL} = X\,\mathrm{Re}_d^2 + r \qquad \textbf{Equation 10}$$

$$X = \frac{\mu}{\rho c} \qquad \textbf{Equation 11}$$

$$\mathrm{Re}(Z)^*_{NL} = \mathrm{Re}_d\, Md + r \qquad \textbf{Equation 12}$$

$$\mathrm{Re}(Z)^* = \frac{1}{\rho c}\left[\frac{\sqrt{8\upsilon\omega}}{\varepsilon c}\left(1+\frac{t}{d}\right)\right] + \left(\mathrm{Re}_d\,.M.d + r\right) \qquad \textbf{Equation 13}$$

Linear Non-linear

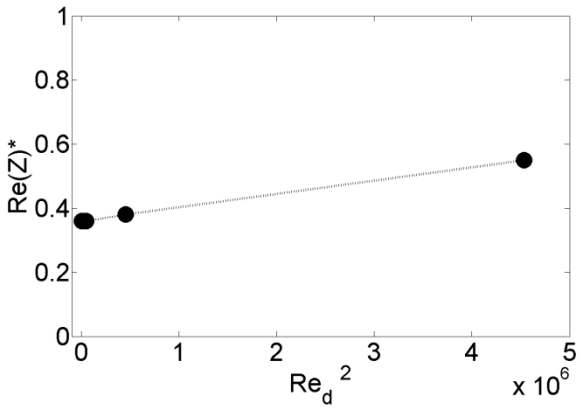

Figure 12 – Measured resistance (Re(Z)*) of HSPL_ARRAY #1 at the resonant frequency over the SPL range 125dB to 155dB against the square of the Reynolds number (Re_d^2).

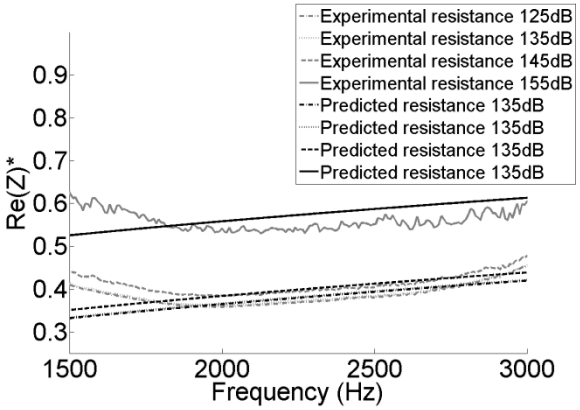

Figure 13 – Experimental and predicted resistance (Re(Z)*) for HSPL_ARRAY #1 using the proposed semi-empirical model over the SPL range 125dB to 155dB

2.2.4 Effect of the grazing flow within a cavity on the attenuation performance of a resonant array

The high SPL aspect is not the only differentiating factor between the cavity environment and the room environment from which resonant arrays are typically used. Therefore, it is of interest to investigate how the low velocity grazing flow experienced by array when installed into a cavity may affect their attenuation performance. It was not possible to experimentally assess the effect of grazing flow across the resonant array faceplate due to the limitation of the impedance measuring equipment. However, as all of the possible array positions within a cavity experience a grazing flow it is important to comment on the possible effects grazing flow may have on the attenuation performance characteristics. Previous investigations into the effect of grazing flow on the attenuation performance of resonant arrays have shown that a grazing velocity will provide a small increase in the resistance of an array [15]. Several studies have concluded that the increase in array resistance due to grazing flow ($\mathrm{Re}(Z)^*_{GF}$) can be accounted for using the term in *Equation 14*, where K is a constant (K=0.3 [20] or K=0.53 [21]) and M is the grazing flow Mach number. The value of resistance related the grazing flow (*Equation 14*) is summed with the resistance terms in *Equation 13* (see *Equation 15*). For a typical array as used in this study with a porosity of ε=8.7% and with a grazing Mach number of M=0.3 the effect of grazing flow is expected to be negligible with values of the normalised resistance ($\mathrm{Re}(Z)^*_{GF}$) between 0.0025 and 0.0043. As the effect of grazing flow is predicted to be negligible and no experimental data is available to confirm the values predicted this term will not be used within the analytical model used for the prediction of the performance of the resonant arrays used within this study.

$$\mathrm{Re}(Z)^*_{GF} = \frac{KM}{\rho c \varepsilon} \qquad \textbf{Equation 14}$$

$$\Sigma \mathrm{Re}(Z)^* = \mathrm{Re}(Z)^* + \mathrm{Re}(Z)^*_{GF} \qquad \textbf{Equation 15}$$

3 Results and Discussion

3.1 Summary of previously reported 1/40th scale tests

A series of preliminary tests were completed using a small scale (1/40th) cavity model at Cranfield University. The tests investigated the attenuation performance from two resonant arrays and three porous mesh devices and the results were previously reported within the interim report [1]. This section will provide a short summary of the findings from these initial tests. The geometric and acoustic properties of the devices shown can be found in the interim report [1]. A full summary of all the attenuation results is provided in *APPENDIX A*.

3.1.1 Resonant arrays

ARRAY A (*Table 1*) was designed to attenuate the 2nd mode at around 2kHz and was designed with a specific value of 0.33 for the normalised faceplate resistance. This resistance value was chosen based on the trend between high 2nd mode attenuation and faceplate resistance levels of around Re(Z)*=0.3 [1]. With *ARRAY A* installed into the front wall of the model cavity an attenuation of 15dB at the 2nd mode was achieved. This reduced the modal peak from 159dB to 144dB and also yielded an OASPL reduction of 2dB for Mach 0.9 flow (*Figure 14a*). This result confirms that an array with a resistance of 0.33 can achieve a high level of attenuation for the second mode. This result supports the design of the medium scale arrays TGF_0.7_1 and TGF_1.5_1 which are designed to have a specific impedance within the range that demonstrates the largest attenuation performance within the small scale tests.

ARRAY B (*Table 1*) was designed to target the third mode at around 3.2kHz with a faceplate that exhibits low resistance characteristics. A low resistance array was chosen based on previous small scale (1/40th) tests which indicate that the third mode is best attenuated by arrays with a normalised resistance lower than 0.1 [1]. With *ARRAY B* installed into the cavity rear wall provided a notable attenuation of 19dB at Mach 0.9 (*Figure 14b*). One consequence of the third mode attenuation is the increase in the amplitude of the second mode (*Figure 14b*). The phenomenon of second mode amplification accompanying third mode attenuation has been seen consistently throughout the 1/40th scale tests and also been demonstrated for other cavity palliatives [22]. The phenomenon known as “peaking” involves the redistribution of energy between the cavity modes from one mode to another receptive mode. This results in the OASPL of the cavity not being attenuated and in some cases being increased by around 4dB. The effect of peaking and the link to mode switching within the cavity is discussed in the *section 3.2.* This result supports the design of the medium scale arrays TGF_0.7_2 and TGF_1.5_2 as these were both designed to target the third cavity modes with specific low values of resistance (Re(Z)*).

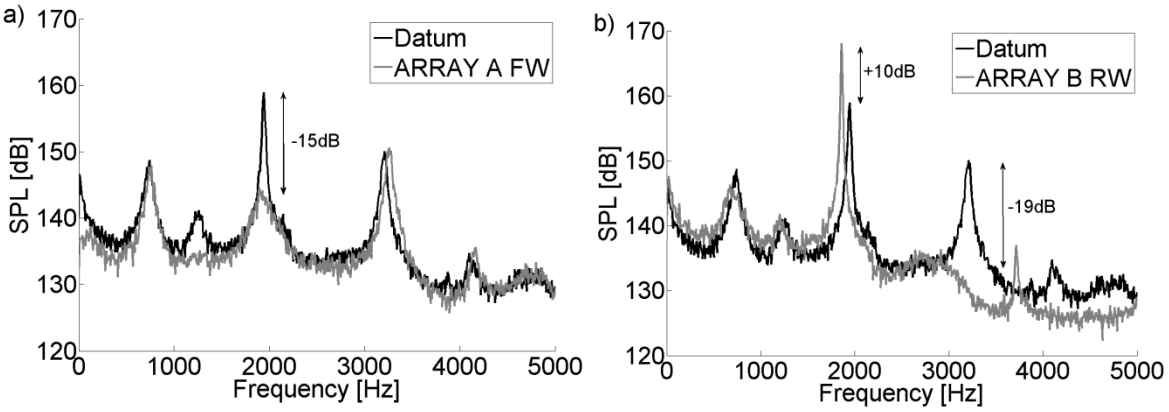

Figure 14 – Small scale attenuation results from a) ARRAY A installed in the front wall, b) ARRAY B installed in the cavity rear wall. (at Mach 0.9)

3.1.2 Porous mesh devices

The porous mesh devices were expected to provide a broadband attenuation and affect multiple modal peaks with the greatest attenuation for higher frequencies within the spectrum. *MESH A* yielded the largest attenuation (12dB (*Figure 15*)) although this was limited to the third mode and frequencies above 4kHz. The attenuation provided by the mesh arrays was limited to the frequencies where the mesh faceplate exhibited the highest resistance with values of the normalised mesh resistance (Re(Z)*) estimated to be around 0.6 based on impedance tube results [1].

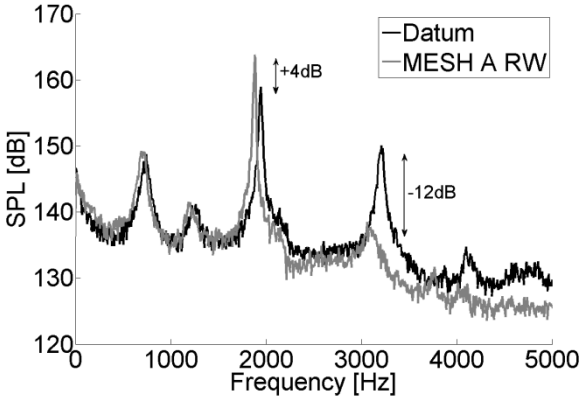

Figure 15 – Small scale attenuation results from MESH A installed in the cavity rear wall (at Mach 0.9).

3.2 Mode switching within the spectra of resonant cavities

To investigate the underlying cause of the spectral peaking effect, where the attenuation of one mode coincides with the simultaneous amplification of another mode, the time history for several test cases were analysed using a short term Fourier transform (STFT). A STFT differs from the Fourier transform routine which is used throughout this study in that it performs a Fourier transform routine on a small portion of a data set. By splitting the data in this way the frequency content of the data can be analysed at discrete time steps and the evolution of the dynamic phenomena can be captured in both the frequency and time domains. The STFT method requires a trade-off between the temporal and frequency resolutions. This trade-off is controlled by the values of the sample/window size and the window overlap. The sample/window size was set at 2^{10} and the overlap was set at 2^{9}. These values resulted in resolutions of 0.0064s for the temporal case and 78.13Hz for the frequency case. Whilst, this frequency resolution is around 20 times less than that used for the spectral analysis it is equivalent to 6.5% of the frequency separation of the individual modes. This enables the individual modes to still be identified by their frequency. However, due to the larger frequency resolution the peak values for the modal SPL will differ between the spectrogram and the typical spectral plots. The data from this process is plotted as a carpet plot with time on the x-axis, frequency on the y-axis, and contours coloured by SPL.

The phenomenon of peaking has been discussed in previous studies relating to other cavity palliatives [22]. Peaking involves the redistribution of energy between the cavity modes from one mode to another receptive mode. This mode switching behaviour has been demonstrated within open cavity flows at low (<Mach 0.1) and medium (Mach 0.4) Mach number flows [23] [24]. *Figure 16a* shows the spectrogram from the STFT analysis of the small scale datum cavity flow at Mach 0.95. The three prominent Rossiter modes are seen as the dark horizontal bands at frequencies of around 750Hz, 2kHz, and 3.2kHz where the darker colour corresponds to a higher SPL intensity. In this case the mode switching phenomena is present for the second and third modes. Periods of high intensity of the third mode coincide with periods of low intensity for the second mode and periods of high intensity for the second mode coincide with periods of low intensity at the third mode. This is denoted by the solid vertical lines enclosed by arrows. To highlight this effect the same data is re-

plotted with defined cut on threshold levels for the individual modes (*Figure 16b*). This creates a plot where a point is only made when the modal intensity increases over a defined level. *Figure 16b* provides a clearer indication of the mode switching behaviour between the second and third modes. The intermittency of the first mode does not appear to be related to the occurrence of either the second or third Rossiter modes.

The correlation between the time histories for the individual modes was investigated to examine if the mode switching between the second and third modes could be identified. It was expected that the second and third modes would exhibit a strong negative correlation coefficient as this is associated with 180° out of phase systems, which is the case for modal switching. The correlation coefficients between the first three cavity modes are given in *Table 8* and these confirm the strong negative correlation between the second and third modes with a coefficient of -0.61. This large correlation value is in contrast to the values between the other cavity modes which are all low and indicate that there is no mode switching involving the first mode.

When a large attenuation was demonstrated at either the second or third Rossiter mode the intensity of another mode within the cavity spectrum was seen to increase. It is proposed that this increase in the modal intensity is related to the switching of energy between the modes. *Figure 17* shows the STFT spectrograms for the cases of targeting the second (*Figure 17a*) and third (*Figure 17b*) Rossiter modes which resulted in peaking. These plots show that for a cavity with an array configuration the intermittency of the modes is removed and the mode which undergoes the peaking effect becomes dominant for all time steps within the sample. The targeted attenuation of a mode appears to impede the modal receptivity to the switching energy within the cavity and instead of the energy being spread between several modes it is limited to a single frequency and this limiting of the energy dispersal manifests as the increase in modal amplitude of a non targeted mode seen in *Figure 14b.*

When the second mode was targeted peaking of the third mode only occurred at Mach 0.95. However, when the third mode was targeted peaking occurred at all subsonic Mach numbers tested. Within the small scale cavity datum spectrum the second mode is dominant with an SPL of around 164dB. The third mode has the second largest intensity with and SPL of around 150dB. Therefore, the receptivity of a mode is thought to be related to the intensity level of a mode. If a mode has an SPL below a certain threshold that mode will no longer receive the shared energy and peaking will occur. For instance, a small attenuation at the third mode will reduce the modal SPL to a relatively low level and the mode may no longer be receptive to the shared energy, but the same attenuation level at the second mode may result in the modal intensity remaining above the critical threshold value and so the mode is still receptive to the shared energy. In this example case the attenuation of the third mode would result in peaking as the energy cannot be accepted by the third mode. However, the attenuation of the second mode will not stop the mode accepting the shared energy and would not be expected to cause peaking within the spectrum. The shared energy can also be thought of as the total energy associated with the modal generation process and this energy is spread between the cavity modes during the generation process.

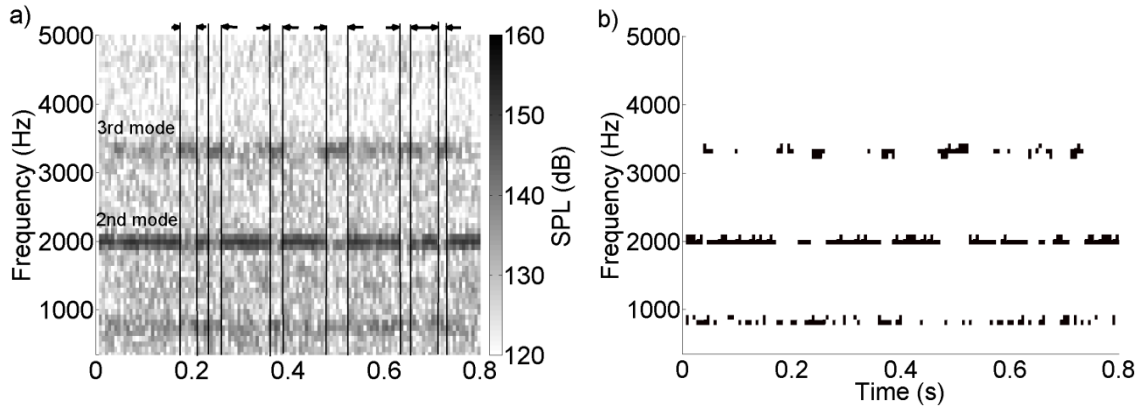

Figure 16 – a) Datum spectrogram for Mach 0.95 freestream flow (vertical lines enclosed by arrows indicate mode switching periods), b) Datum spectrogram for Mach 0.95 freestream flow with cut on levels defined for individual modes to highlight mode switching (threshold levels: 1st= 137dB, 2nd=145dB, 3rd=140dB).

	1st mode	2nd mode	3rd mode
1st mode	1.00		
2nd mode	-0.16	1.00	
3rd mode	0.15	-0.61	1.00

Table 8 – Correlation coefficients between the first three Rossiter modes for the small scale cavity at Mach 0.95.

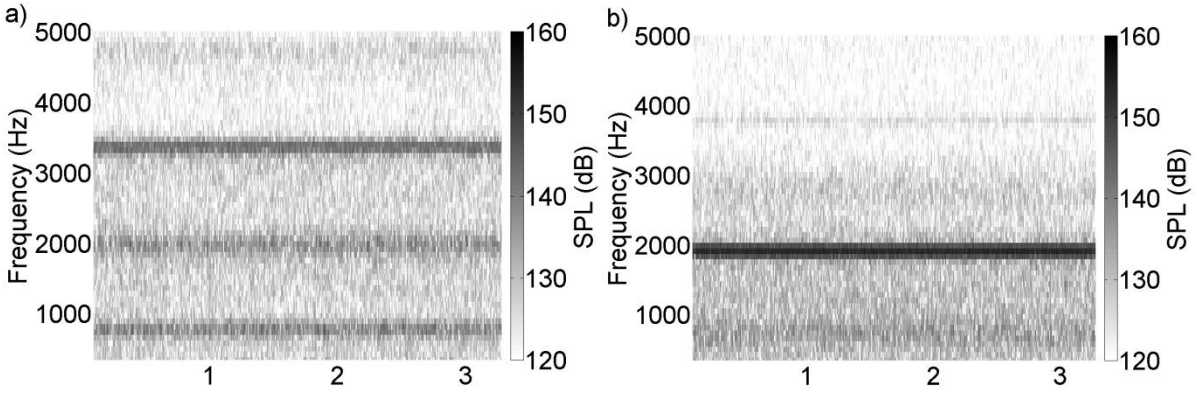

Figure 17 – Spectrogram for cavity configuration at Mach 0.95 with a) ARRAY A FW, b) ARRAY B RW

3.3 Medium scale (1/20th) palliative investigation

A series of medium scale (1/20th) wind tunnel tests were carried out using a generic cavity model installed into the TGF at Wright Patterson Air Force Base in Ohio. These tests support the main objective of this investigation into cavity palliatives and also provide additional research opportunities which were not available within the facilities at Cranfield University. The additional research opportunities include the ability to test the palliative performance in a larger 1/20th scale cavity and also under supersonic (Mach 1.5) freestream conditions. A brief description of this facility is provided in *section 2.1.2* of this report and a detailed description is provided in the accompanying interim report [1].

3.3.1 Subsonic test results at Mach 0.7

A series of medium scale wind tunnel investigations were carried out using resonant arrays (*Table 3*) installed within the ADDICT cavity model at a freestream Mach number of 0.7. This section summarises the main results from these tests and the full attenuation results are included in *Appendix A*.

3.3.1.1 Datum modal characteristics for the medium 1/20th scale cavity model

As the 1/20th scale testing took place in a different facility and at a different Mach number (Mach 0.7 compared to Mach 0.8-0.95) the modal characteristics within the cavity differ somewhat from the 1/40th scale case. The SPL spectra over the cavity ceiling for the 1/20th scale cavity at Mach 0.7 are shown in *Figure 18a*, where the vertical dashed lines correspond to the predicted Rossiter frequencies (*Equation 1*). The spectrum displays two clear modal peaks with the peaks at 800Hz and 1250Hz corresponding to the second and third Rossiter modes respectively. The experimental Rossiter modes occur within 5% of the frequencies predicted by *Equation 1*. The spectra cropped to these modes are shown in *Figure 18b* and *Figure 18c* respectively. No modes are present at frequencies higher than the third mode and the broadband noise level decreases rapidly from 135dB at 2kHz to around 125dB at 5kHz. Unlike with the 1/40th scale case, the third mode is dominant within the 1/20th scale cavity (*Figure 18*). At 1/20th scale the third mode exhibits a narrow peak with a width of around 200Hz. However, the second mode exhibits a wider peak with a width of around 400Hz. The second mode also consists of multiple split peaks. It is expected that the narrow third mode can be successfully attenuated using resonant arrays. However, the wider second mode may not be suitable for attenuation from the targeted approach offered by resonant arrays. The following sections will discuss the results from the resonator tests at Mach 0.7. The SPL of both modes typically increases by around 15dB from the front of the cavity to the rear (*Figure 18a*). The modal shapes correspond well to the predicted shapes (*Figure 19*) [25] (see *section 3.3.1.1*). It is expected that little or no attenuation will be exhibited at the transducer locations which correspond to the modal pressure nodes as the reduced pressure at this point will not improve the resistance characteristics of the arrays (see *section 2.2*) [1]. For the second mode these positions are at x/l of 0.20 and 0.65 and for the third mode the nodes are at an x/l of 0.2, 0.5, and 0.8.

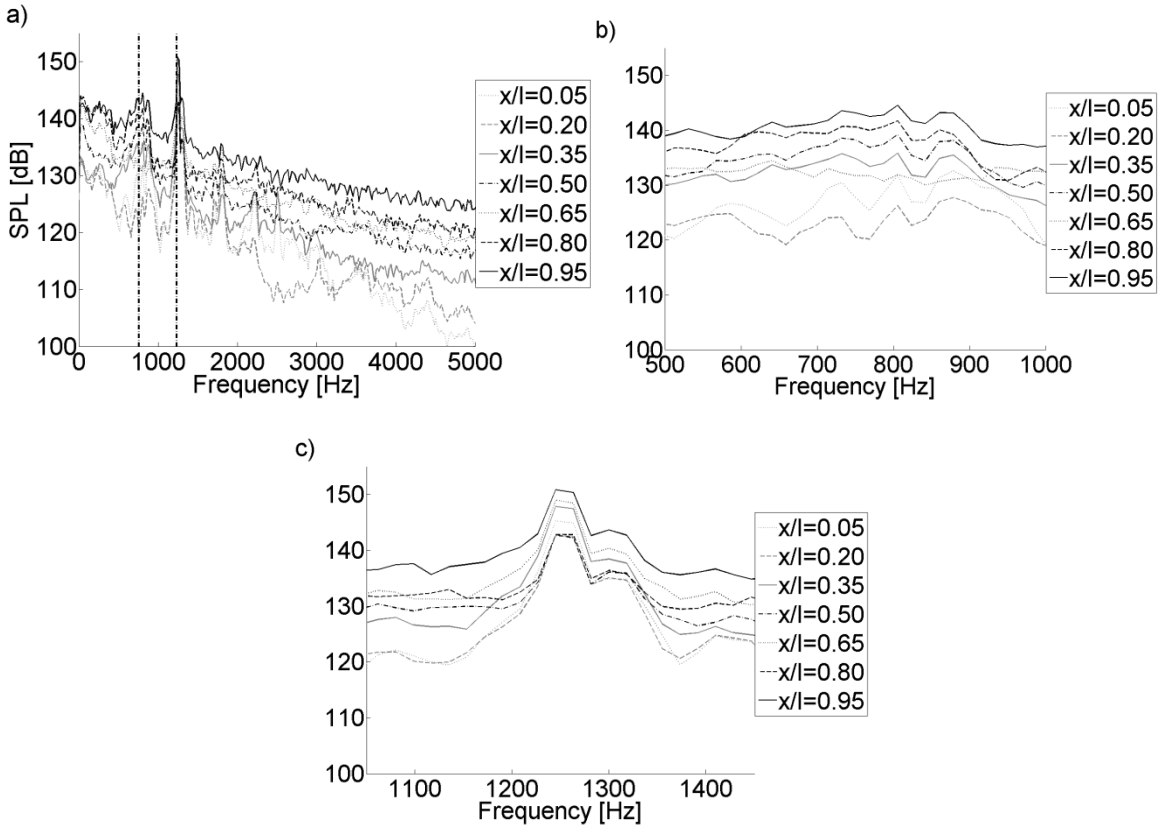

Figure 18 – a) Datum cavity spectrum for the ADDICT cavity model at Mach 0.7 at each transducer location (vertical dashed lines correspond to predicted Rossiter modal frequencies (*Equation 1*)), b) Datum cavity spectrum for the ADDICT cavity model at Mach 0.7 cropped to the second mode only, c) Datum cavity spectrum for the ADDICT cavity model at Mach 0.7 cropped to the third mode only.

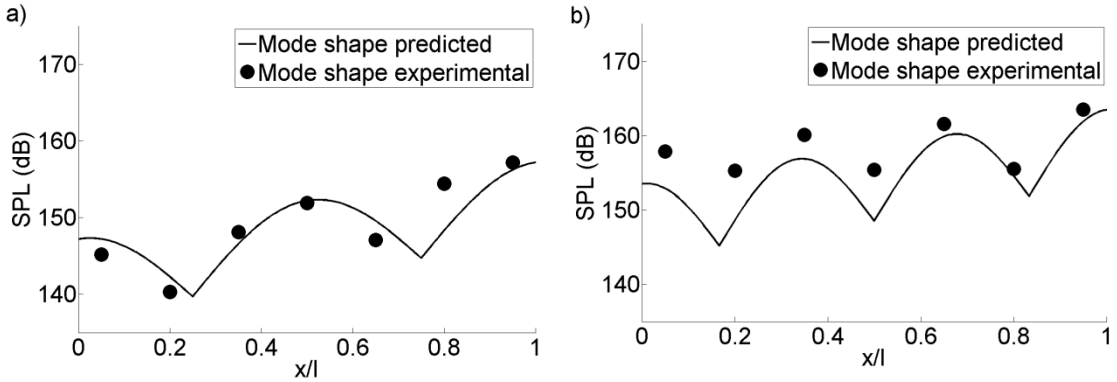

Figure 19 – a) Predicted and experimental mode shape for the second mode within the ADDICT cavity model at Mach 0.7, b) Predicted and experimental mode shape for the third mode within the ADDICT cavity model at Mach 0.7

3.3.1.2 Targeted attenuation of the second mode

Following the successful attenuation of the second mode within the small (1/40th) scale tests an array (TGF_0.7_1) was designed to target the second mode within the medium scale (1/20th) cavity. TGF_0.7_1 was designed following the same principles as ARRAY 2-1 [1]. However, due to the lower Mach number (Mach 0.7 compared to Mach 0.8-0.95 for the 1/40th scale cases) and the different modal characteristics it was unknown if a resonant array would be a suitable palliative for the second mode within the 1/20th scale case. *Figure 20* shows that TGF_0.7_1 has no effect on the cavity SPL for the front wall configuration. The same disappointing result was also exhibited for the rear wall configuration. Across the cavity ceiling there was no attenuation exhibited for either the front or rear wall configurations. Therefore, this test case demonstrates that the modal characteristics of the ADDICT cavity at Mach 0.7 cause difficulties for successful resonant array attenuation. Due to the low Mach number (Mach 0.7) the SPL of the targeted modal peak is relatively low (around 144dB (*Figure 20*)) which is also expected to have a detrimental effect on the resistance properties of the array and therefore reduce the ability to attenuate. The wideband and split nature of the second mode are also not ideal for targeting with resonant arrays as the devices only offer narrowband attenuation. For the ADDICT cavity spectrum this is not a major issue as the dominant third mode has a narrow peak which is suitable for resonant array attenuation. A problem may arise if the dominant modal peak exhibited a split or wideband peak as this could not be treated through the use of resonant array based palliatives. This case of a wideband dominant mode demonstrates the limits in which a resonant array based palliative can be successfully used. A designer would need to assess the bandwidth of the dominant modal peaks prior to designing resonant arrays as the attenuation from resonant arrays may not be as robust as a spoiler type palliatives under subsonic conditions. The source of this wide peak in the ADDICT spectra is investigated along with the possibility of mode switching within the subsonic ADDICT cavity in *section 3.3.1.5.*

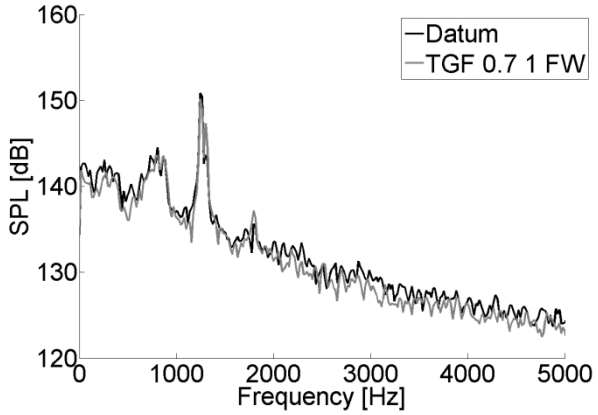

Figure 20 – Spectrum comparison with TGF_0.7_1 in front wall (FW) at Mach 0.7. (Transducer x/l=0.95)

3.3.1.3 Targeted attenuation of the third mode

A high level of attenuation has been demonstrated at the third mode within the small (1/40th) scale cavity [1] and TGF_0.7_2 was designed following a similar design principle to the small scale test cases [1]. However, due to the different spectral characteristics of the medium scale cavity, notably the split second mode and the dominant third mode, it was unknown if an array designed based on the small scale findings would provide a comparable high level of attenuation.

Figure 21a shows that TGF_0.7_2 achieved an attenuation of around 4dB at the third mode within the medium (1/20th) scale cavity. This attenuation is much lower than that exhibited for the small scale test cases, where attenuation levels were up to 15dB for a similar device at Mach 0.9. However, it was expected that testing at a lower Mach number would result in lower attenuation levels due to the lower acoustic pressure within the cavity at the lower Mach numbers. An

attenuation of up to 8dB was typical across the cavity ceiling for the rear wall configuration (*Figure 21b*). For the front wall configuration attenuation levels on the ceiling near to the front wall (x/l=0.05 and x/l=0.2) improved to around 10dB. However, attenuation across the remaining cavity ceiling was of a level similar to the rear wall case. For both front and rear wall configurations there was around 3dB of broadband attenuation exhibited at frequencies at and above the third mode (*Figure 21a*). In a similar manner to the small scale tests when the third mode was targeted the second mode exhibited peaking (*Figure 21a*). The cause of this peaking effect within the small scale cavity at Mach 0.95 was discussed in *section 3.2* and is investigated for the medium scale cavity at Mach 0.7 in *section 3.3.1.5*.

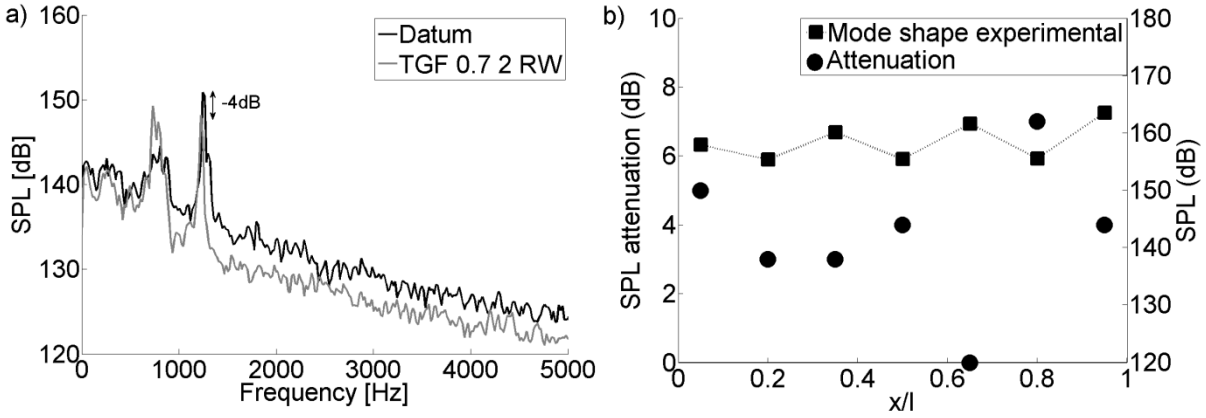

Figure 21 – a) Attenuation from TGF_0.7_2 in the rear wall (RW) at Mach 0.7. (Transducer x/l=0.95), b) Attenuation from TGF_0.7_2 over the cavity ceiling with experimental mode shape plotted on the secondary axis for Mach 0.7.

3.3.1.4 Can the poor attenuation at low Mach number (Mach 0.7) be improved by combined installation?

No attenuation of the second cavity mode at 800Hz was exhibited when the second mode was targeted with a single resonant array configuration (*Figure 20*). Therefore it was decided to investigate the attenuation that was exhibited at the third mode through a combined configuration using an array which did exhibit some useful attenuation. This combined configuration placed TGF_0.7_2 at both the front and rear wall of the cavity. This combined approach improved the attenuation on the ceiling at x/l=0.95 from 4dB up to 9dB (*Figure 22a*) and also improved the attenuation near the front wall (x/l=0.05) up to around 15dB (*Figure 22b*). However, the improved attenuation of the third mode led to significant peaking at the second mode (*Figure 22a*), which was typically amplified by around 12dB. This combined installation produced an overage OASPL attenuation of around 2dB over the cavity ceiling. Therefore, combined resonant array configurations can improve on the poor attenuation of single configurations at low Mach number. However, this improvement in the attenuation of one mode may be offset against the amplification of another mode within the spectrum. Indeed, when a second and third mode array were used in combination attenuation levels of around 5dB were exhibited at both the second and third mode as the peaking effect was counteracted (See *Appendix A.2* (*Table 14*)).

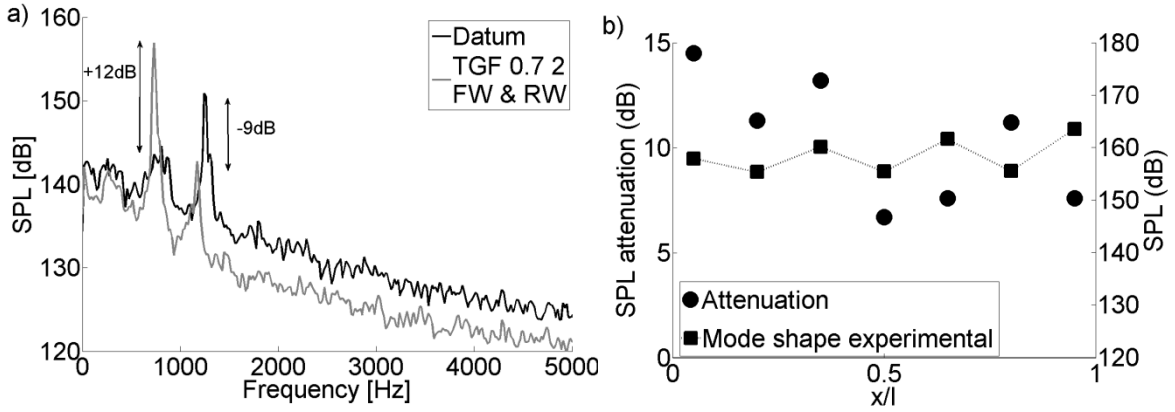

Figure 22 – a) Attenuation from the combined installation of TGF_0.7_2 in the front and rear cavity walls at Mach 0.7 (transducer x/l=0.95), b) Attenuation of the third mode from TGF_0.7_2 across the cavity ceiling with experimental mode shape at Mach 0.7.

3.3.1.5 Investigation of mode switching within the ADDICT cavity under subsonic conditions (Mach 0.7)

It was of interest to assess whether the peaking exhibited by the installation of certain arrays within the ADDICT cavity model (see *section 3.3.1.4*) was caused by the same mechanisms as within the small scale cavity (see *section 3.2*). A short term Fourier transform (STFT) routine was carried out on data samples taken from the medium scale wind tunnel tests to investigate the underlying physics behind the modal spectra. A STFT investigation of the data from the small scale cavity tests revealed the phenomenon of mode switching between the cavity modes (see *section 3.2*). This phenomenon, where large pressure intensity at one mode coincides with a drop in intensity at another mode, has also been reported for other cavities at different scales and freestream conditions [22] [23] [24] . The STFT was conducted using a window length of 2^{10} and an overlap of 2^{9}, both of these resulted in a temporal resolution of 0.0068s and a frequency resolution of 73.2Hz. As there is a trade-off between a high temporal resolution and a low frequency resolution the modal peaks become smeared as the energy content is effectively averaged over a wider frequency range. This has the effect of altering the frequencies at which the modes occur, but because the resolution is lower than the modal separation it is not expected to affect the data. The peak SPLs for the modal peaks are also expected to be lower than for the standard SPL spectra due to this smearing process.

Figure 23a shows the STFT profile for the datum cavity at Mach 0.7. In this plot (*Figure 23a*) the third mode can be clearly identified by the dark horizontal band at around 1.4kHz. Due to the wide and split nature of the second modal peak this is hard to distinguish from the background noise. However, a series of high intensity disturbances are present around 800Hz. This figure does not show the clear mode switching which was present within the small scale cavity. However, it does demonstrate that the energy within the modes is intermittent as neither the second or third mode are constant for the duration of the sample length (*Figure 23b*).

This lack of switching behaviour is also investigated through a correlation analysis of the modal time histories and the correlation coefficient values are given in *Table 9*. The main observation is that the coefficient values are all low and in particular the value between the second and third mode does not indicate a strong relationship, unlike for the small scale case where mode switching was evident (*Table 8*). The values in *Table 9* support the conclusion that there is no strong mode switching relationship within the ADDICT cavity model at Mach 0.7.

Figure 23c demonstrates the peaking effect, where energy that would be present at one mode appears at another mode. In this case (*Figure 23c*) the third mode was targeted with attenuation and this resulted in peaking at the second mode. The peaking within the STFT plot is exhibited as both an increase in the modal intensity at the second mode as well as an increase in the proportion of the

sample for which the mode is present. This result is consistent with the effects that were exhibited for the small scale cavity tests (see *section 3.2*).

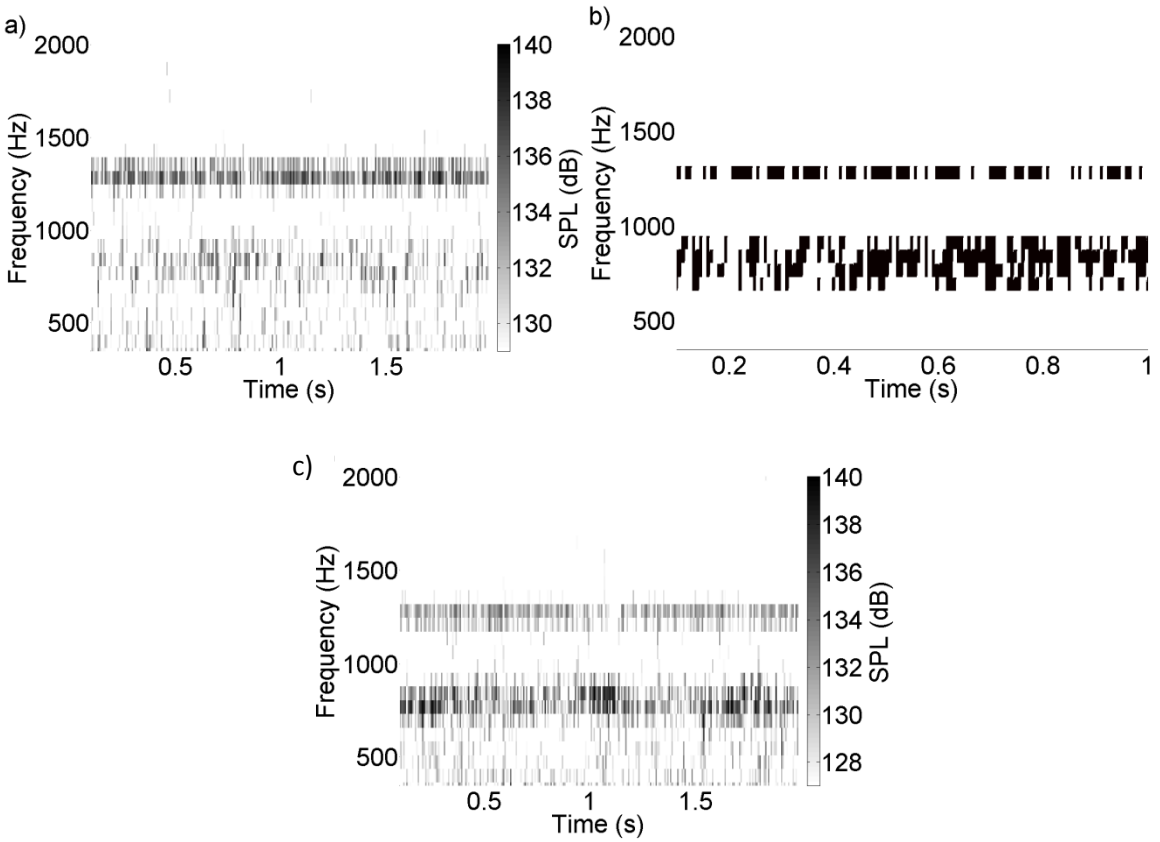

Figure 23 – a) Datum spectrogram for Mach 0.7 freestream flow over the ADDICT cavity model, b) Datum spectrogram for Mach 0.7 freestream flow with cut on levels defined for individual modes to highlight mode intermittency (threshold levels: 2nd=128dB, 3rd=133dB). c) Spectrogram for Mach 0.7 freestream flow over the ADDICT cavity model with TGF_0.7_2 installed in the rear wall.

	1st mode	2nd mode	3rd mode
1st mode	1.00		
2nd mode	0.03	1.00	
3rd mode	-0.08	-0.24	1.00

Table 9 – Correlation coefficients between the first three Rossiter modes for the medium scale cavity at Mach 0.7.

3.3.2 Supersonic tests results at Mach 1.5

The typical passive control choice for operational cavities is a full width spoiler installed upstream of the cavity. Indeed, previous investigations have shown attenuations of around 20dB for solid spoilers at high subsonic Mach numbers [3]. However, while the attenuation performance of a spoiler may increase with increasing Mach number within the subsonic regime the attenuation performance from spoilers decreases with increasing supersonic Mach numbers and in some cases can lead to a significant increase in the modal intensities [3] [26]. Above Mach 1.3 increases in modal intensities of around 15dB have been demonstrated by previous experiments [3] which could cause additional damage to the stores and aircraft. Therefore, an alternative attenuation approach is required for supersonic flight conditions. It was therefore of great interest to assess whether resonant arrays could provide useful attenuation levels under supersonic conditions.

It should be noted that the following tests were conducted using the TGF at Wright Patterson Air Force Base (*section 2.1.2*) as the Cranfield University 2.5" wind tunnel is not capable of achieving supersonic condition with the cavity liners installed. These tests were conducted using the ADDICT cavity model which is roughly 1/20th scale and exhibits open flow characteristics [27] [28] (section 2.1.1).

3.3.2.1 Datum modal characteristics for the medium scale cavity at Mach 1.5

The subsonic medium scale cavity did not display the ideal modal characteristics for resonant array attenuation (see *section 3.1*). Whilst the cavity was modal the second mode had a broad split peak with a low SPL which would not typically be suitable for attenuation by a narrowband resonant device. However, despite this, the spectrum from the supersonic case exhibits promising modal characteristics (*Figure 24*). A series of modal peaks are present within the spectrum with the first three Rossiter modes exhibiting the highest SPLs at around 500Hz, 1.2kHz, and 2kHz (*Figure 24a*). The peaks for the second and third modes occur within 10% of the frequencies predicted by *Equation 1* (*Figure 24a*). The relative levels of the modal peaks are similar to those exhibited within the small scale cavity at subsonic Mach numbers with the second mode exhibiting the highest SPL with a peak value of around 153dB (x/l=0.95)(*Figure 24b* and *Figure 24c*) (see *section 3.1*). Both the second and third modal peaks have a width of 200Hz and are therefore ideal for targeted attenuation from resonant arrays. The following section discusses the effects of targeted modal attenuation of the second and third modes.

The ADDICT cavity mode has seven dynamic pressure transducers located across the cavity ceiling [1] and this enables the modal characteristics to be examined throughout the cavity. For both the second and third modes the SPL typically increases by around 15dB as x/l increases from 0.05 to 0.95 (*Figure 25*). The measured SPL at each transducer location provides information relating to the mode shapes within the cavity and these compare favourably to the shapes predicted analytically (*Figure 25*). From the spectra the peak SPL relating to each mode can be plotted against x/l position on the ceiling to produce the plots showing the shape of the modes within the cavity (*Figure 25*). The analytical mode shapes were predicted using a semi empirical model, which requires the SPL at the rear wall of the cavity and the cavity l/h aspect ratio [25]. It is expected that when the attenuation properties are investigated the low levels of attenuation will be exhibited at the locations near to the pressure nodes. This link between attenuation and modal SPL is related to the increase in resistance of an array at higher SPLs (see *section 2.2*) [1]. The second mode exhibited two pressure nodes around positions of x/l of 0.2 and 0.8 (*Figure 25a*). The third mode exhibits three pressure nodes at positions of x/l around 0.2, 0.5, and 0.8 (*Figure 25b*). These mode shapes are similar to those exhibited by organ pipe resonances where a system of standing waves are set up confined by closed ends.

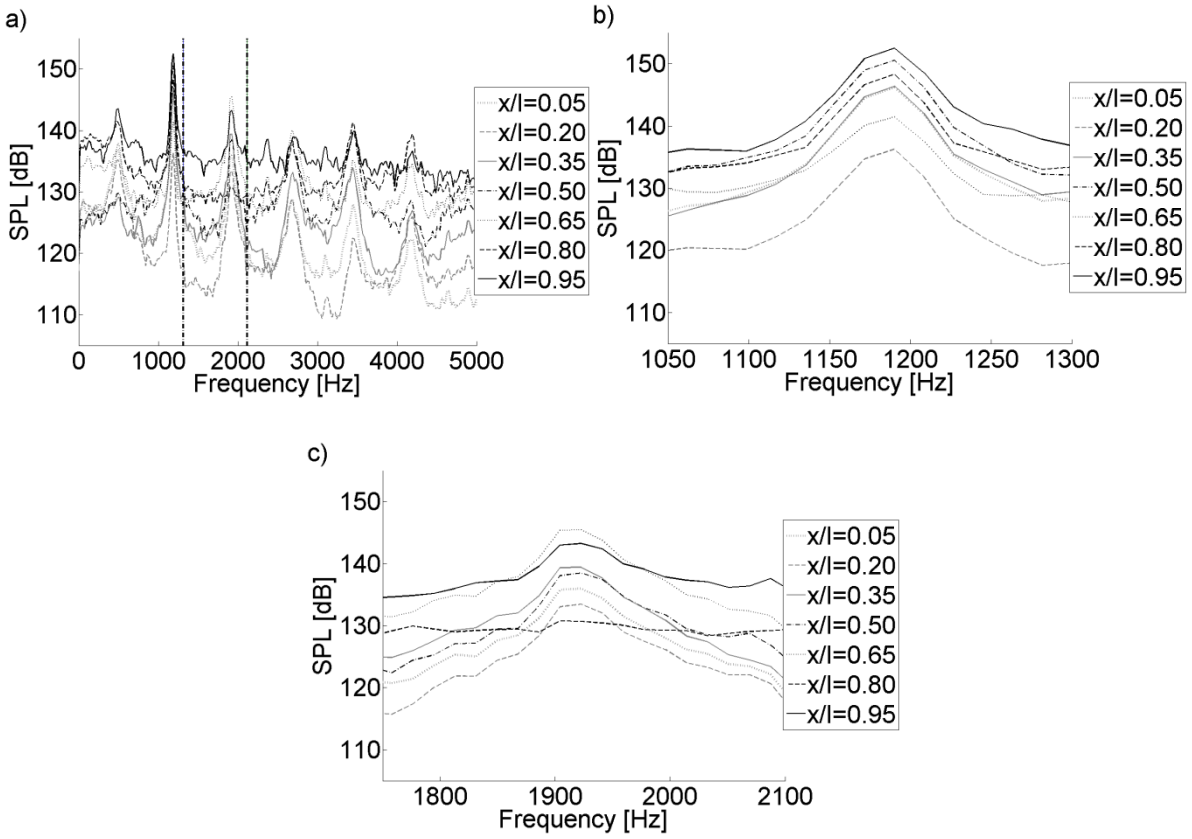

Figure 24 – a) Datum cavity spectra for the ADDICT cavity at Mach 1.5 (vertical lines indicate predicted Rossiter frequencies from *Equation 1),* b) Datum SPL spectra for the ADDICT cavity at Mach 1.5 cropped to the second mode, c) Datum SPL spectra for the ADDICT cavity at Mach 1.5 cropped to the third mode.

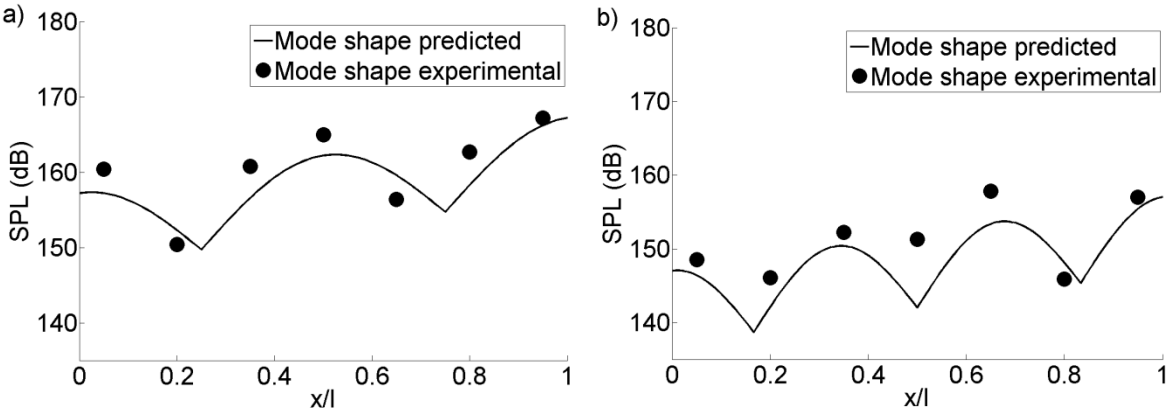

Figure 25 – a) Predicted and experimental mode shape for the second mode within the ADDICT cavity at Mach 1.5, b) Predicted and experimental mode shape for the third mode within the ADDICT cavity at Mach 1.5.

3.3.2.2 Effect of targeted modal attenuation

The primary mode of operation for a single resonant array is to attenuate a targeted modal peak. The small scale wind tunnel tests have demonstrated that resonant arrays can successfully attenuate targeted modal peaks under subsonic conditions. However, there is currently no evidence of the performance of resonant array under supersonic conditions and therefore it was of interest to investigate whether a similar level of attenuation could be achieved for a supersonic test case. Previous tests using spoiler type palliatives have shown a decrease in the attenuation performance under supersonic conditions [3]. Therefore, if resonant arrays can provide a reasonable level of attenuation under supersonic conditions they would demonstrate a potential for use as complementary palliatives for use in conjunction with spoilers under supersonic speeds.

Figure 26 shows that targeted modal attenuation can be achieved for supersonic (Mach 1.5) freestream conditions. TGF_1.5_1 (*section 2.1.2.1*) provided around 10dB of attenuation at the second mode (1.2kHz) (*Figure 26b*). The levels of attenuation follow the SPL mode shape profile for the datum cavity where the larger attenuation levels coincide with the higher modal intensities (*Figure 26b*). As expected there was no attenuation of the broadband noise and no attenuation of non-targeted modes. The levels of attenuation are lower than those demonstrated for the small scale test cases however, this can be explained by the SPL differences between the two cavities. The small scale cavity exhibited modal SPLs that were around 10dB higher than those within the ADDICT model under supersonic conditions (Mach 1.5). An increase in SPL of around 10dB corresponds to around a threefold increase in the acoustic pressure and an increase in SPL has also been linked to improved attenuation due to the increase in the resistance of the array (*section 2.2*) [1]. Therefore, a higher attenuation would be expected at a pressure anti-node location for instance the cavity end wall locations.

Figure 27 demonstrates that the targeted attenuation approach from resonant arrays can also be used to attenuate the third mode. TGF_1.5_2 provided 10dB attenuation at the rear of the cavity ceiling and up to 26dB of attenuation at the front of the cavity ceiling (*Figure 27b*). The large variation in modal attenuation over the cavity ceiling is partially due to the varying modal SPL over the cavity length. At each transducer location the third mode SPL was reduced to the surrounding broadband level. However, due to the modal peak being around 26dB higher than the broadband noise level at the x/l=0.05 position this resulted in a higher level of attenuation compared with the modal attenuation at the x/l=0.95 position (*Figure 27b* and *Figure 27c*). Results from the small scale tests also confirm that typically a higher level of attenuation is exhibited in the forward section of the cavity [29]. This effect may also be linked to the direction of the waves which are related to the individual modal peaks.

Notably, there is no peaking, where attenuation at one mode leads to an amplification at another mode, exhibited for the third mode attenuation under supersonic conditions (*Figure 27a*). This may be related to the different modal characteristics when compared with the subsonic small scale test cases. For the subsonic medium scale cases, where peaking is evident (*section 3.3.1*) there are only the first three modes present in the spectrum, however under supersonic conditions eight peaks are present. Therefore, for the supersonic case there are a greater number of peaks which could receive the energy that is re-distributed from the third mode. As the energy is distributed over a wider range of peaks the change in SPL that would normally be associated with this (peaking) is not evident as the mode switching can still continue with a large number of cavity modes. The effect of mode switching within the cavity under supersonic conditions is examined in *section 3.3.2.4*. Also the attenuation of the third mode reduced to low levels at a position of x/l=0.8 as this position coincides with a pressure node for the third mode (*Figure 27b*) The low SPL at the pressure node is expected to reduce the attenuation as the array are not expected to reduce the modal peak below the broadband noise levels as they are typically narrowband devices.

Another effect of targeted attenuation at the third mode is a shift in frequency in one or more of the other modes within the spectrum *Figure 27a* and *c*. The change in modal frequency due to at the attenuation from a resonant array is limited to cases where the third mode is attenuated and is seen at both small (1/40th) and medium (1/20th) scale. Often in these cases the second mode undergoes a slight (3%) drop in resonant frequency, but all other modes remain close to their datum frequencies. Under supersonic conditions (Mach 1.5 (1/20th scale)) some higher frequency modes undergo a small (<1%) increase in their modal frequency when the third mode is attenuated. A drop in frequency would typically be associated with an extension of the cavity length (l), possibly attributable to the array backing cavities. However, both increases and decreases in modal frequencies are exhibited (*Figure 27a* and *c*). Therefore, if these changes in modal frequency were due to the simple effect of the increased cavity length, it is expected that these frequency changes would occur for all modes in all of the cases with an array installed even if no attenuation occurred or when the second mode was targeted. However, this is not the case and therefore another mechanism may be behind the frequency changes.

The target cavity mode and non-target modes will interact with the palliatives differently due the arrays impedance properties. At resonance the magnitude of the total array impedance (|Z|) is comprised solely of the arrays resistance (Re(Z)*). For all cases Re(Z)* at resonance was predicted to be less than the characteristic impedance (Z_0=ρc) (soft boundary), which would result in an out of phase reflection from the surface coupled with an attenuation of the incoming wave. However, a wave at a non-resonant frequency would encounter the array with a $|Z|>Z_0$ (rigid boundary), which causes an in-phase reflection with no attenuation. Therefore, the non-target modes are expected to encounter the perforated wall as a rigid boundary, which would act in a similar manner as the datum solid cavity walls. This explains why for the majority of cases the non-target modal frequencies are unaffected by the installation of an array. One subtlety, which may explain why the third mode arrays cause the reduction in the second modal frequency is that they were typically designed with a low resistance (Re(Z)*) and a high porosity (ε). It is expected that these devices would not provide the same rigid boundary condition as the second mode devices, due to the large open area of the faceplate. Therefore, waves associated to the generation of the other modes may pass through the faceplate and effectively extend their travel within the cavity.

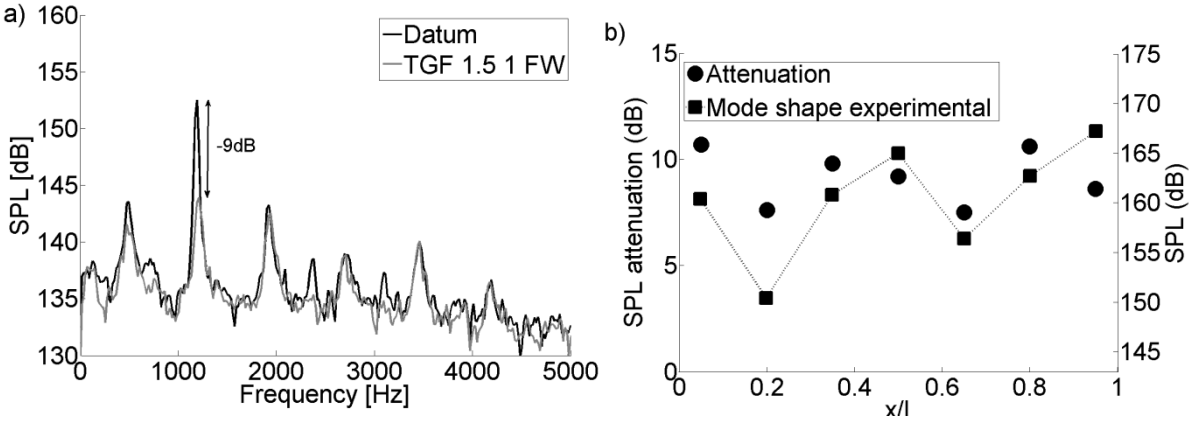

Figure 26 – a) Targeted attenuation of the second mode with TGF_1.5_1 in the front wall (transducer x/l=0.95), b) SPL attenuation of the second mode against x/l position on cavity ceiling with experimental second mode shape plotted against secondary y-axis. (Mach 1.5).

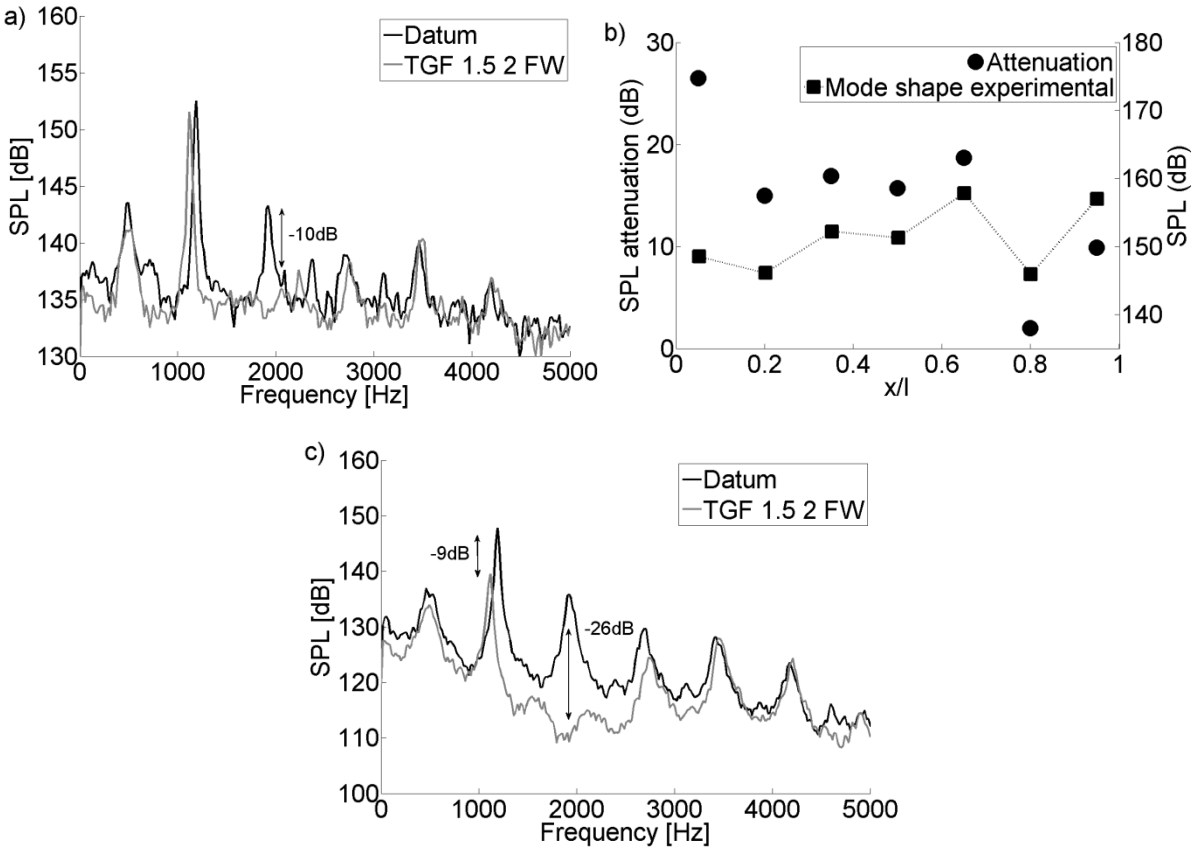

Figure 27 – a) Targeted attenuation of the third mode with TGF_1.5_2 in the front wall (transducer x/l=0.95), b) SPL attenuation of the third mode against x/l position on cavity ceiling with experimental third mode shape plotted against secondary y-axis, c) Targeted attenuation of the third mode with TGF_1.5_2 in the front wall (transducer x/l=0.05) (Mach 1.5).

3.3.2.3 Effect of combined resonant array configurations

A high level of attenuation under supersonic conditions has been demonstrated at the second and third modes from individual arrays tuned to the separate modal frequencies (*Figure 26* and *Figure 27*). It was therefore of interest to investigate whether a combined resonator configuration would both improve single mode attenuation and broadband attenuation in a similar fashion to the results from the small scale combined configuration [1].

The medium scale cavity was configured with TGF_1.5_1 (*section 2.1.2.1*) in the front wall and TGF_1.5_2 in the rear wall. This placed the second mode array in the favoured front wall position and the third mode array in the rear wall. This set up has demonstrated high levels of peak and broadband attenuation within the small scale tests under subsonic conditions [1]. This configuration provided around 10dB of attenuation at the second mode (*Figure 28*) which reduces the second mode from around 151dB to 141dB. An average OASPL reduction over the cavity ceiling of 7dB was also exhibited by this configuration. The SPL at the third mode frequency was reduced by around 15dB from 145dB to 130dB (*Figure 28a*). A broadband attenuation of around 6dB was also exhibited by the combined configuration and this is consistent with what was expected from the subsonic test cases (*Figure* 22). Attenuation levels across the cavity ceiling were more constant than for the individual cases, both the attenuation level at the second and third modes were around 10dB

throughout the cavity with the largest attenuation levels coinciding with the higher modal SPLs at the rear end of the cavity (*Figure 28b*). As with the individual third mode case the attenuation of the third mode is reduced at the position x/l=0.8 as this coincides with a pressure node for the third mode (*Figure 25*). Typically, the levels of attenuation have followed the modal shapes across the cavity ceiling. This is expected as the mechanism behind the attenuation from a resonant array is linked to the pressure of the environment in which it is operated (*section 2.2*) [1].

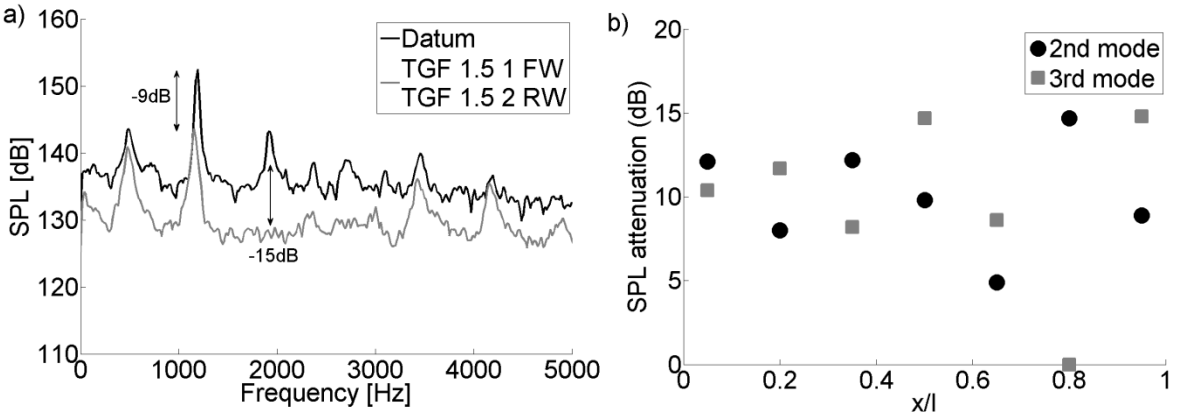

Figure 28 – a) Attenuation form the combined configuration of TGF_1.5_1 in the front wall (FW) and TGF_1.5_2 in the rear wall (RW), b) SPL attenuation of the second and third modes against x/l position on the cavity ceiling. (Mach 1.5).

In summary, resonant arrays have demonstrated a potential for use as cavity palliatives under supersonic flow conditions. Peak attenuation levels within the cavity of up to 26dB have been shown at single modes for both single and combined array configuration. This is an important result as alternative palliative devices such as spoilers do not typically provide high attenuation levels under supersonic conditions. If resonant arrays were to be used in combination with an upstream spoiler it is expected that high levels of attenuation could be achieved over a wide range of Mach numbers. This would enable an aircraft fitted with the palliative combination to operate its weapon bay within a greater portion of its flight envelope without causing damage to the aircraft or the carried stores.

3.3.2.4 Investigation of mode switching within the ADDICT cavity under supersonic conditions (Mach 1.5)

Under subsonic conditions there was no evidence of mode switching within the medium scale cavity. However, the energy within the cavity modes was shown to be intermittent (see *section 3.3.1.5*). The STFT profile for the supersonic case also demonstrates that the cavity modes are not constant for the length of the data sample and that there is a certain amount of intermittency (*Figure 29a*). Unlike for the small scale cavity case there is no evidence of mode switching between the second and third cavity modes under supersonic conditions within the medium scale cavity (*Figure 29b*).

The correlation relationship between the first three cavity modes was investigated and the correlation coefficient values are given in *Table 10*. It was expected that the correlation coefficient values between all of the modes would be low as the spectrogram data (*Figure 29*) does not indicate a clear mode switching relationship. Low correlation coefficients were exhibited between all three of the cavity modes with values typically around 0.05 (*Table 10*). These low correlation coefficient values confirm that there is not a clear mode switching relationship within the ADDICT cavity model under supersonic (Mach 1.5) conditions.

Within the spectra for the medium scale cavity under supersonic condition there are 6 clear modal peaks (*Figure 24*). Therefore, it is expected that the energy within the cavity modes is shared constantly between all of the modes. This switching between modes, some of which have low peak

SPLs, makes it difficult to detect the relationship between the occurrence of each mode within the sample time. However, despite this the results do demonstrate the intermittency which explains the effect of peaking caused by certain palliative devices (see *section 3.2* and *3.3.1.5*).

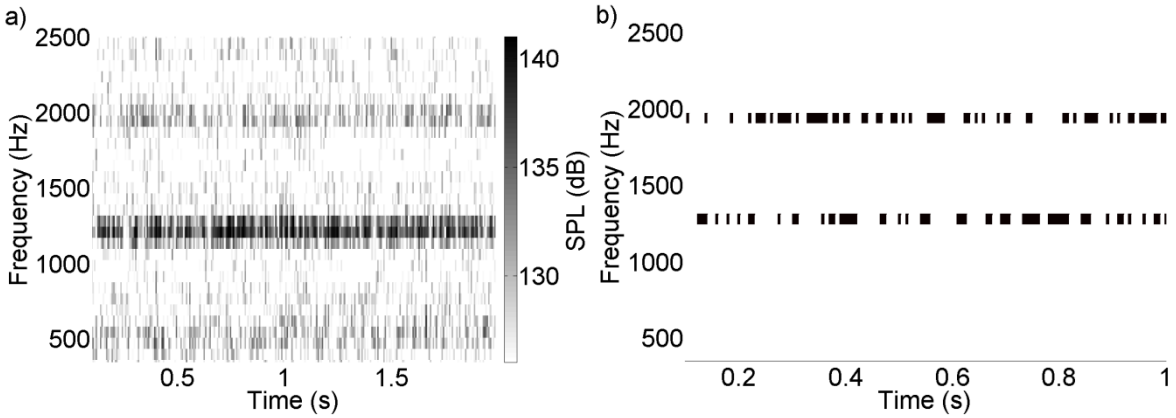

Figure 29 – a) Datum spectrogram for Mach 1.5 freestream flow within the ADDICT cavity model, b) Datum spectrogram for Mach 1.5 freestream flow with cut on levels defined for individual modes to highlight mode intermittency (threshold levels: 2^{nd}=133dB, 3^{rd}=129dB).

	1^{st} mode	2^{nd} mode	3^{rd} mode
1^{st} mode	1.00		
2^{nd} mode	-0.06	1.00	
3^{rd} mode	0.04	-0.05	1.00

Table 10 – Correlation coefficients between the first three Rossiter modes for the medium scale cavity at Mach 1.5.

4 Conclusions

- Resonant arrays have demonstrated large peak attenuation levels of up to 26dB under supersonic (Mach 1.5) freestream conditions in a 1/20th scale cavity model.

- Combined resonator configurations under supersonic (Mach 1.5) conditions have provided simultaneous attenuation at multiple modes with peak attenuation levels of up to 15dB with up to 7dB OASPL attenuation.

- Under subsonic conditions (Mach 0.8 to 0.95) 1/40th scale resonant arrays designed using resistance as a performance prediction metric have provided attenuation levels of up to 19dB.

- Porous mesh based devices have also demonstrated a useful amount of attenuation (12dB) within a 1/40th scale cavity.

- The introduction of ventilation to the backing cavity of a porous wire mesh based device reduces the amount of attenuation provided by the device.

- The analytical model used for the design of the resonant arrays is not acceptable for use within the high SPL cavity environment and a new semi-empirical modal has been proposed to account for the non-linear effects of the high SPL within a cavity environment.

- Evidence of the intermittency and switching tendencies of the cavity modes has been demonstrated within both the 1/20th and 1/40th scale cavities at Mach 0.7, 1.5 and Mach 0.95 respectively. This evidence supports the mechanism for modal peaking where attenuation at one mode caused an amplification of another mode.

5 References

[1] Roberts, D., & MacManus, D. (2012). *Attenuation of cavity bay noise -- Interim report -- EOARD award #: FA8655-11-1-3025.* Cranfield University.

[2] Rossiter, J. (1966). Wind-Tunnel Experiments on the Flow over Rectangular Cavities at Subsonic and Transonic Speeds. *ARC-R&M-3438* .

[3] Shaw, L., & Shimovetz, R. (1994). *Weapons bay acoustic environment AGARD-CP-549.*

[4] ESDU. (2006). Aerodynamics and aero-acoustics of rectangular planform cavities. Part II: Unsteady flow and aero-acoustics 04023.

[5] Heller, H., Holmes, D., & Covert, E. (1971). Flow-Induced Pressure Oscillations in Shallow Cavities (Supersonic Wind Tunnel Study of Flow Induced Pressure Oscillations in Shallow Rectangular Cavity, investigating Resonant Frequencies and Pressure Mode Shapes). *Journal of Sound and Vibration , 18* (545-553).

[6] ESDU. (2009). Aerodynamics and aero-acoustics of rectangular planform cavities. Part IIIB: Alleviation of unsteady flow effects - acoustic suppression using passive devices 08012.

[7] Cattafasta III, L. N., Williams, D. R., Rowley, C. W., & Alvi, F. S. (2003). Review of Active Control of Flow-Induced Cavity Resonance. *AIAA 2003-3567* .

[8] Kook, H., Mongeau, L., & Franchek, M. A. (2002). Active Control of Pressure Fluctuations Due To Flow Over Helmholtz Resonators. *Journal of Sound and Vibration , 255(1), 61-76*.

[9] D'Antonio, P., & Cox, T. J. (2005). *Technical bulletin on the design od microperforated transparent absorbers.* Upper Markboro, MD: RPG Diffuser Systems Inc.

[10] Hsu, J., & Ahuja, K. (1996). Cavity Noise Control Using Helmholtz Resonators. *AIAA 96-1675* .

[11] Roberts, D., & MacManus, D. (2011). *Weapon bay noise attenuation - Final report. CDE contract no RT/COM/7/053. .* Cranfield University.

[12] Cox, T. J., & D'Antonio, P. (2004). *Acoustic Absorbers and Diffusers.* Spon Press.

[13] Saladin, J. (2006). *Shakedown & determination of tunnel control setting for refurbished trisonic gasdynamic facility (TGF).* AFRL-VA-WP-TR-2007-3015.

[14] Pratt & Whitney Aircraft. (1967). *A study of the suppression on combustion osicllations with mechanical damping devices (NASA contract# NA$8-11038).*

[15] Guo, Y., & Åbom, M. (2006). *Acoustic properties of new design elements for cooling systems -- micro-perforated panels.* European Commission DG Research.

[16] Dickey, N., Selamet, A., & Novak, J. (2000). The effect of high-amplitude sound on the attenuation of perforated tube silencers. *Journal of the Acoutic Society of America , Vol: 108* (Iss: 3).

[17] Guess, A. (1975). Calculation of perforated plate liner parameters from specified acoustic resistance and reactance. *Journal of Sound and Vibration , vol: 40* (iss: 1).

[18] Maa, D. (1994). Microperforated panel at high sound intensity. *Proceeding of internoise.* Yokohama.

[19] Tayong, R., & Leclaire, P. (2010). Hole interaction effects under high medium sound intensities for micro-perforated panels design. *10ème Congrès Français d'Acoustique.* Lyon.

[20] Rice, E. (1973). *A model for the pressure excitation spectrum and acoustic impedance of sound absorbers in the presence of grazing flow.* NASA TM-X-71418.

[21] Rao, N., & Munjar, M. (1986). Experimental evalutation of impedance of perforates with grazing flow. *Journal of the Acoustical Society of America , vol: 108* (iss: 2).

[22] Williams, D., Rowley, C., Colonius, T., Murray, R., MacMartin, D., Fabris, D., et al. (2002). Model-based control of cavity oscillations -- Part 1: Experiments AIAA 2002-0971.

[23] Lusseyran, F., Pastur, L., & Letellier, C. (2008). Dynamical analysis of an intermittency in an open cavity flow. *Physics of Fluids , vol: 20*.

[24] Kergerise, M., Spina, E., Garg, S., & Cattafesta III, L. (2004). Mode-switching and nonlinear effects in compressible flow over a cavity. *Physics of Fluids , vol: 16* (iss: 3).

[25] Smith, D., Shaw, L., Talmadge, R., & Seely, D. (1974). *Aero-acoustic environment of rectangular cavities with length to depth ratios of five and seven.* AFFDL-TM-74-79-FYA.

[26] Dix, R., & Bauer, R. (2000). *Experimental and theoretical study of cavity acoustics AEDC-TR-99-4.* Arnold Engineering Development Center.

[27] Schmit, R., McGaha, C., Tekell, J., Grove, J., & Stanek, M. (2009). Performance results for the optical turbulence reduction cavity AIAA 2009-702.

[28] Schmit, R., Semmelmayer, F., Haverkamp, M., & Grove, J. (2001). Fourier analysis of high speed shadowgraph images around a Mach 1.5 cavity flow field, AIAA 2011-3961.

[29] Roberts, D., & MacManus, D. (March 2010). *Weapon bay noise attenuation Interim report 1 RT/COM/7/053.* Cranfield University.

6 List of Symbols, Abbreviations, and Acronyms

d	Orifice diameter (mm)
D	Orifice pitch spacing (mm)
t	Orifice length/faceplate thickness (mm)
t'	Orifice length/faceplate thickness including end corrections (mm)
L	Backing length (mm)
ε	Faceplate porosity (%)
α	Absorption coefficient ($0<\alpha<1$) or constant in Rossiter's equation
β	Bandwidth normalised by resonant frequency (%)
ρ	Density (kgm^{-3})
c	Speed of sound (ms^{-1})
m	Mass (kg) or Rossiter mode number
k	Wavenumber (m^{-1}) or constant in Rossiter's equation
ω	Radial frequency ($rads^{-1}$)
Z	Impedance (Nsm^{-3})
l	Cavity length (m)
w	Cavity width (m)
h	Cavity depth (m)
x	Position ordinate along cavity length
y	Position ordinate from cavity centreline
z	Position ordinate along cavity depth
u_o	Particle velocity within orifice (ms^{-1})
u_n	Particle velocity normal to orifice/faceplate (ms^{-1})
M	Mach number
Re_d	Reynolds number through orifice (based on orifice diameter (d))
p_{ref}	SPL reference pressure ($2x10^{-5}Pa$)
Z_0	Characteristic impedance (ρc)
Im	Imaginary
Re	Real
FW	Front wall
RW	Rear wall
*	Normalised

Appendix A: Experimental results summary

This appendix provides a summary of all of the attenuation results from the various palliative devices tested under EOARD award number FA8655-11-1-3025. The results are presented in terms of the attenuation of the SPL peaks for the second and third cavity modes as these are the dominant modes for both the small and medium scale test cases. The attenuation of the OASPL is also included for comparison, however, it should be noted that due to the narrow operating bandwidth of the resonant arrays the OASPL attenuations are expected to be lower than those demonstrated for alternative palliatives such as spoilers.

A.1 1/40th scale device attenuation results

Device	Position	Mach number	2nd mode attenuation (dB)	3rd mode attenuation (dB)	OASPL attenuation (dB)
ARRAY A	FW	0.8	9	0	2
ARRAY A	FW	0.9	15	0	2
ARRAY A	FW	0.95	16	+6	3
ARRAY A	RW	0.8	8	5	3
ARRAY A	RW	0.9	8	2	3
ARRAY A	RW	0.95	7	0	3
ARRAY B	FW	0.8	+5	10	0
ARRAY B	FW	0.9	+6	15	+2
ARRAY B	FW	0.95	+5	13	+1
ARRAY B	RW	0.8	+14	10	+4
ARRAY B	RW	0.9	+10	19	+4
ARRAY B	RW	0.95	+7	16	+2
MESH A	FW	0.8	+8	5	+1
MESH A	FW	0.9	+10	10	+2
MESH A	FW	0.95	+1	6	0
MESH A	RW	0.8	+9	8	+1
MESH A	RW	0.9	+4	12	+1
MESH A	RW	0.95	+6	14	+1
MESH B	FW	0.8	+2	4	2
MESH B	FW	0.9	+8	10	+1
MESH B	FW	0.95	0	10	1
MESH B	RW	0.8	0	6	3
MESH B	RW	0.9	0	4	2
MESH B	RW	0.95	0	6	1
MESH C	FW	0.8	+5	0	1
MESH C	FW	0.9	0	0	0
MESH C	FW	0.95	4	2	3
MESH C	RW	0.8	+4	7	1
MESH C	RW	0.9	+4	10	0
MESH C	RW	0.95	3	10	0

Table 11 – Peak SPL and OASPL attenuation results for the individual small scale palliative devices tested over the Mach number range Mach 0.80 to 0.95. Attenuations quoted for reference transducer located on the cavity ceiling at a position of x/l=0.95.

A.2 1/20th scale device attenuation results for Mach 0.7

		2nd mode attenuation (dB)							3rd mode attenuation (dB)							OASPL attenuation (dB)						
		x/l							x/l							x/l						
Device	Position	0.05	0.2	0.35	0.5	0.65	0.8	0.95	0.05	0.2	0.35	0.5	0.65	0.8	0.95	0.05	0.2	0.35	0.5	0.65	0.8	0.95
TGF_0.7_1	FW	0	0	0	0	0	0	0	0	0	0	0	0	0	0	1.2	0.5	0.8	1	0.5	0.6	0.6
TGF_0.7_2	FW	+5	+4	+5	+5	0	+5	+5	8.5	5.6	10.9	0	0	1.8	1.8	2.6	1.8	3.5	0.3	2.7	0.8	0.9
TGF_0.7_3	FW	0	0	0	0	0	0	0	0	0	0	0	0	0	0	1.4	0.6	1.2	1.3	0.8	0.6	0.7
TGF_0.7_4	FW	0	0	0	0	0	0	0	3	3	3	3	3	3	3	1.4	0.4	1.1	1.4	1	0.8	0.9
TGF_0.7_5	FW	0	0	0	0	0	0	0	0	0	0	0	0	0	0	0.6	0.3	0.5	0.7	0.2	0.2	0.1
TGF_0.7_7	FW	+2	0	+2	+2	0	+2	+2	4	3	4	2	2	2	2	2	1.3	2.5	1.2	1.9	0.9	1.1
TGF_0.7_2	RW	+4	+1	+4	+6	0	+4	+5	5	3	3	4	0	7	4	2.5	2.2	1.8	1	1.3	0.9	1.3
TGF_0.7_3	RW	0	0	0	0	0	0	0	0	0	0	0	0	0	0	1.5	1.2	1.6	1.2	0.9	0.9	1.2

Table 12 – Peak SPL and OASPL attenuation results for the individual medium scale resonant array palliative devices tested at Mach 0.70.

		2nd mode attenuation (dB)							3rd mode attenuation (dB)							OASPL attenuation (dB)						
		x/l							x/l							x/l						
Device	Position	0.05	0.2	0.35	0.5	0.65	0.8	0.95	0.05	0.2	0.35	0.5	0.65	0.8	0.95	0.05	0.2	0.35	0.5	0.65	0.8	0.95
TGF_m1	RW	0	0	0	0	0	0	0	0	0	0	0	0	0	0	1.2	1	1	0.9	0.6	0.9	1.2
TGF_m2	RW	+3.7	+2.3	+2	+4.9	0	+2.8	+4.3	0	0	0	0	0	0	0	1.3	1	0.6	0.8	0.3	0.7	1
TGF_m3	RW	6.1	4.2	1.8	0	0	2	2	2.3	1.9	1	2	0	9.8	1	2.6	2.2	1.8	2	1	2	2

Table 13 – Peak SPL and OASPL attenuation results for the individual medium scale porous mesh based palliative devices tested at Mach 0.70.

		2nd mode attenuation (dB)							3rd mode attenuation (dB)							OASPL attenuation (dB)						
		x/l							x/l							x/l						
Device FW	Device RW	0.05	0.2	0.35	0.5	0.65	0.8	0.95	0.05	0.2	0.35	0.5	0.65	0.8	0.95	0.05	0.2	0.35	0.5	0.7	0.8	0.95
TGF_0.7_2	TGF_0.7_2	+12.3	+9	+11.7	+13.3	+7.9	+11.8	+11.6	14.5	11.3	13.2	6.7	7.6	11.2	7.6	1.9	3.6	2.5	+1.6	2.7	+0.5	+0.1
TGF_0.7_4	TGF_0.7_2	4.3	2.3	3.6	5.5	0	4	5.1	5	3.8	2.2	6.6	0	6.5	3.6	2.9	2.5	2.2	2	1.7	1.6	2
TGF_0.7_2	TGF_0.7_4	+2.9	1.3	+2.9	+5.9	0	+3.1	+3.8	12.3	9.2	14.4	2.8	7	6.7	5.2	4.2	3.2	5.3	1.8	3.9	2.1	2.5

Table 14 – Peak SPL and OASPL attenuation results for the combined configurations of medium scale resonant array palliative devices tested at Mach 0.70.

A.3 1/20th scale device attenuation results for Mach 1.5

		2nd mode attenuation (dB)							3rd mode attenuation (dB)							OASPL attenuation (dB)						
		x/l							x/l							x/l						
Device	Position	0.05	0.2	0.35	0.5	0.65	0.8	0.95	0.05	0.2	0.35	0.5	0.65	0.8	0.95	0.05	0.2	0.35	0.5	0.65	0.8	0.95
TGF_1.5_1	FW	12.2	9	11	10.7	8.3	10.9	9.8	2.6	1.6	1.3	3.4	1.7	0	1.8	3.3	1.1	2.8	2.7	1.4	1.5	1.4
TGF_1.5_2	FW	2.9	9	1.7	3.3	9.9	1.7	1.8	24.7	12.4	8	9.9	12	4	8.5	2.3	1.7	1.7	2.2	2.4	1.2	1.1
TGF_1.5_3	FW	3.1	2.5	3	2.9	3.4	3.2	3	0	0	0	0	0	0	0	1.2	0.5	1	0.9	0.6	0.5	0.5
TGF_1.5_4	FW	2.4	2.5	2.2	2.3	3.5	2.3	1.9	0	0	0	0	0	0	0	1.2	1	1.2	1.4	1.3	1.2	0.7
TGF_0.7_2	FW	13.3	13.5	11.7	13.3	13.3	12	11	6.9	4.3	3.5	9.7	5.2	2	4.7	4	1.6	3.4	3.8	2.4	2.1	1.8
TGF_0.7_7	FW	8.1	6.8	7.4	7.6	6.9	8.2	7.3	0	0	0	0	0	0	0	2	0.4	1.8	2	1.1	0.9	0.9
TGF_1.5_1	RW	6.6	6.2	6.8	6.1	4.7	6.4	8.3	4.2	4.5	3.9	4.3	3.3	0	2.9	3	1.5	3.1	2.8	1.8	1.6	1.9
TGF_1.5_2	RW	0	+1	1	0	+1.6	2	0	9.5	11.5	8.7	10	8.2	0	10.6	1.6	2.5	3.3	1.8	2.9	2.8	1.6
TGF_m3	FW	2	0	0	0	7.8	0	0	7.9	5.1	7.8	8.4	7.8	6.6	5.7	4.2	3.8	3.3	4	5.3	3.6	2.3

Table 15 – Peak SPL and OASPL attenuation results for the individual medium scale palliative devices tested at Mach 1.5.

		2nd mode attenuation (dB)							3rd mode attenuation (dB)							OASPL attenuation (dB)						
		x/l							x/l							x/l						
Device FW	Device RW	0.05	0.2	0.35	0.5	0.65	0.8	0.95	0.05	0.2	0.35	0.5	0.65	0.8	0.95	0.05	0.2	0.35	0.5	0.65	0.8	0.95
TGF_1.5_1	TGF_1.5_2	14.6	10.2	15.2	12	8.3	16.9	11.8	9.5	10.7	7.5	15	7.6	0	14.7	7.9	5.6	8.3	8.3	6.9	6.3	5.4
TGF_1.5_2	TGF_1.5_1	8.2	14.5	7	8.2	12.4	6.6	8.3	26.3	10.5	10.6	12	12.8	5	8.9	5	3	4.5	4.8	4.1	3	3
TGF_0.7_2	TGF_1.5_2	8.4	10.1	7.8	7.4	6.5	9.6	5	18	15.8	14	19	14.6	6.1	13.8	6.7	5.2	7.4	7.3	7.2	6.3	4.8

Table 16 – Peak SPL and OASPL attenuation results for the combined medium scale palliative devices tested at Mach 1.5.